



Enzymatically-degradable hydrogel coatings on titanium for bacterial infection inhibition and enhanced soft tissue compatibility via a self-adaptive strategy

Jin Leng^{a,1}, Ye He^{a,b,1}, Zhang Yuan^a, Bailong Tao^a, Ke Li^a, Chuanchuan Lin^a, Kun Xu^a, Maowen Chen^a, Liangliang Dai^d, Xuemin Li^e, Tony Jun Huang^b, Kaiyong Cai^{a,c,*}

^a Key Laboratory of Biorheological Science and Technology, Ministry of Education, College of Bioengineering, Chongqing University, Chongqing, 400044, China

^b Thomas Lord Department of Mechanical Engineering & Materials Science, Duke University, Durham, NC, 27708, USA

^c Chongqing Key Laboratory of Soft-Matter Material Chemistry and Function Manufacturing, Southwest University, Chongqing, 400715, China

^d Institute of Medical Research, Northwestern Polytechnical University, Xi'an 710072, China

^e Innovative Drug Research Centre, School of Pharmaceutical Sciences, Chongqing University, Chongqing, 401331, China

ARTICLE INFO

Keywords:

Titanium

ZnO

Hydrogel coatings

Anti-bacteria

Fibroblasts

Soft tissue compatibility

ABSTRACT

Ideal percutaneous titanium implants request both antibacterial ability and soft tissue compatibility. ZnO structure constructed on titanium has been widely proved to be helpful to combat pathogen contamination, but the biosafety of ZnO is always questioned. How to maintain the remarkable antibacterial ability of ZnO and efficiently reduce the corresponding toxicity is still challenging. Herein, a hybrid hydrogel coating was constructed on the fabricated ZnO structure of titanium, and the coating was proved to be enzymatically-degradable when bacteria exist. Then the antibacterial activity of ZnO was presented. When under the normal condition (no bacteria), the hydrogel coating was stable and tightly adhered to titanium. The toxicity of ZnO was reduced, and the viability of fibroblasts was largely improved. More importantly, the hydrogel coating provided a good buffer zone for cell ingrowth and soft tissue integration. The curbed Zn ion release was also proved to be useful to regulate fibroblast responses such as the expression of CTGF and COL-I. These results were also validated by *in vivo* studies. Therefore, this study proposed a valid self-adaptive strategy for ZnO improvement. Under different conditions, the sample could present different functions, and both the antibacterial ability and soft tissue compatibility were finely preserved.

1. Introduction

Generally, implant-associated infections (IAI) can be effectively prevented by strict operation standards [1–3]. However, in some exceptional circumstances, such as endogenous pathogens and post-operative secondary infection, IAI still occurs. Implantable materials with a large contact area, relatively stable structure, and trophic components (such as organic materials) will provide ideal platforms for bacteria to adhere, proliferate and colonize, which leads to the failure of implantation and the destruction of natural tissues [4–6]. Medical-used titanium has been deeply applied in orthopedic replacements, cardiovascular stents, and connective tissue integration [7–9]. However, the

broader applications it has, the more likely titanium will be threatened by IAI due to the lack of practical self-antibacterial ability.

To address this issue, many novel antibacterial surface modifications of titanium have been developed [10–12]. The construction of different types of metallic oxides on titanium surfaces is very useful for combating pathogen contamination [13,14]. Among them, zinc oxide (ZnO) becomes very popular due to its potent and broad-spectrum antibacterial activity, no matter for Gram-positive and negative bacteria or even the bacteria with drug-resistance property [15–17]. ZnO possesses multiple antibacterial pathways, including the release of Zn²⁺, the generation of reactive oxygen species (ROS), and some special topological features (such as nanorods) [18]. Although the fabrication of ZnO structure on

Peer review under responsibility of KeAi Communications Co., Ltd.

* Corresponding author. College of Bioengineering Chongqing University, Chongqing, 400044, China.

E-mail address: kaiyong.cai@cqu.edu.cn (K. Cai).

¹ Co-first author: Jin Leng and Ye He contributed equally to this work.

<https://doi.org/10.1016/j.bioactmat.2021.05.001>

Received 16 January 2021; Received in revised form 2 May 2021; Accepted 2 May 2021

2452-199X/© 2021 The Authors. Publishing services by Elsevier B.V. on behalf of KeAi Communications Co. Ltd. This is an open access article under the CC

BY-NC-ND license (<http://creativecommons.org/licenses/by-nc-nd/4.0/>).

titanium has reported some tremendous antibacterial outcomes, a significant concern was also brought up: biosafety. The use of ZnO in biomedicine is a “double-edged sword”, as excessive Zn^{2+} and ROS release can also bring serious adverse effects to cells and tissues [19,20]. Many improving strategies have been proposed recently, but the negative influence of ZnO on different cell types was still enormous [21–23]. The balance between antibacterial efficiency and biosafety was also difficult to be fully achieved. Therefore, how to use tremendous antibacterial activity and maintain relatively low toxicity is an urgent task for utilizing ZnO structure on titanium.

As a widely-used percutaneous implantable material, titanium always faces complicated conditions. To achieve an ideal integration with tissues, titanium needs to get along well with both hard tissues (bone) and soft tissues (muscle, skin, adipose tissue, etc.) [24–26]. Actually, solid researches have been published to improve the soft tissue integration of titanium [27,28]. The strategies which could promote protein absorption, collagen deposition, and skin forming will hold a great significance for titanium improvement, especially in some specific conditions like post-infection reconstruction and wound repair [29,30].

The remarkable mechanical properties endow titanium to be an ideal orthopedic implant. Still, the relatively rigid and two-dimensional surface makes it difficult to have the comparable ability of soft tissue integration with other types of implants such as polymeric hydrogels and scaffolds [31]. Therefore, the combination of polymer materials and titanium is valuable. On the one hand, constructing a 3D network structure on titanium will build a special “buffer zone” between titanium and natural tissues. This buffer zone will induce cell migration and infiltration in the initial phase of implantation. Accompanied with the gradual degradation of the polymers, cells will migrate, proliferate, spread, and secrete various proteins to rebuild their own microenvironments and gradually replace the buffer zone to form a good integration with titanium [32]. On the other hand, the underlying titanium could also be useful when the upper polymers contact natural tissues. Many functional ions, proteins, and peptides can be loaded into titanium and released through the polymer to regulate cell behaviors.

More importantly, constructing polymers (hydrogel coatings) on titanium can ideally alleviate the potential toxicity after any titanium-based treatments. For the ZnO structure on titanium, the hydrogel coatings will control the Zn ion release and reduce the direct contact between materials and cells. Additionally, the toxicity of metal ions always presents a dose-dependent manner. High concentrations of Zn ion will bring detriments to cells, but lower concentrations may be beneficial. Therefore, the hydrogel coatings may provide the possibilities to alleviate the toxicity of ZnO, and be useful to regulate cell behaviors.

The only challenge is how to balance antibacterial activity and biosafety. Hydrogel coatings can effectively improve biosafety by controlling the ion release and reducing the direct contact, but the antibacterial activity may also be impaired. Accordingly, both have antibacterial activity and biosafety requires the hydrogel coatings to be more “smart”, or have the self-adaptive ability. Self-adaptive ability means materials could respond to the chemical or physical cues and make the changes automatically, such as phase transition and the breakage of chemical bonding. These changes will endow materials with multiple functions. Herein, we expected that when under bacterial infection conditions, the hydrogel coatings on titanium can expose the underlying ZnO structure faster to exert the antibacterial activity. When under normal conditions, the hydrogel coatings on titanium will be stable and inhibit the toxicity of ZnO. Previously, inspired by the hyaluronidase (HAase) secretion ability of most of the Gram-positive bacteria, many studies have been reported to modify materials with hyaluronic acid to obtain the enzyme-triggered antibacterial ability [33, 34]. Hyaluronic acid is widely distributed in connective tissues of mammals and is bio-compatible. Hence it is suitable to be used as building blocks of biomaterials. Therefore, hyaluronic acid and its derivative may be valuable to construct the hydrogel coatings on titanium. HAase will degrade the coatings when bacteria exist.

In this study, a hybrid hydrogel coating was prepared by mixing methacrylated gelatin (GelMA) and methacrylated hyaluronic acid (HAMA). GelMA could provide excellent bio-compatibility, and the addition of HAMA will give the enzymatically-degradable ability to the hydrogel coating when bacteria exist. To stably construct the hydrogel coating on titanium, we referred to the method reported by Khademhosseini’s group [35]. To graft catechol motifs on the chains of GelMA, and it was capable of adhering to titanium surfaces. Then a ZnO nanoflower-like structure was fabricated on titanium by a hydrothermal method. The stability of the adhesive hydrogel coating on the ZnO structure was explored. Next, the enzymatical degradation ability, Zn ion and ROS release profile, short-term and long-term antibacterial abilities and cell responses were studied. Based on the self-adaptive strategy, the fabricated sample presented different functions under different conditions. When under bacterial infection, the hybrid hydrogel coating was expected to effectively combat bacterial infections. When under the normal condition, the hydrogel coating was stable and the toxicity of ZnO can be largely reduced. Furthermore, cell responses and soft tissue compatibility can also be significantly improved (Scheme 1).

2. Materials and methods

2.1. Materials

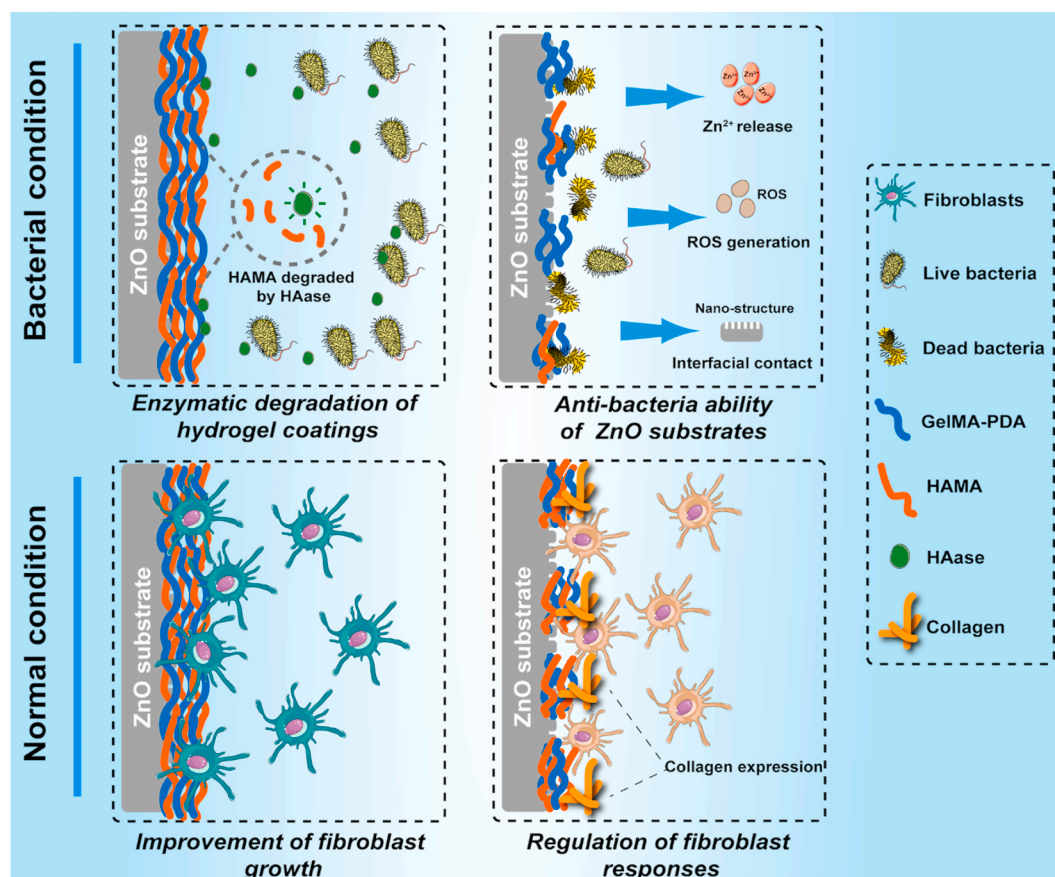
All the experimental titanium samples were commercially-available pure Ti foils (purity: 99.5%) purchased from Alfa Aesar Co. (Tianjin, China). Hoechst 33258, rhodamine-conjugated phalloidin, fluorescein diacetate (FDA), propidium iodide (PI), dopamine hydrochloride, photoinitiator 1-[4-(2-hydroxyethoxy)-phenyl]-2-hydroxy-2-methyl-1-propan-1-one (Irgacure 2959), gelatin (from porcine skin type A) and methacrylic anhydride (MA) were purchased from Sigma-Aldrich Chemical Co. (St. Louis, MO, USA). N, N-Dimethylformamide (DMF), Sodium hyaluronate (HA, 200 kDa) and zinc nitrate hexahydrate were bought from Aladdin Industrial Co. (Shanghai, China). Cell counting kit-8 (CCK-8) was purchased from Beyotime Biotechnology Co. (Jiangsu, China). Rabbit polyclonal antibody Collagen I was obtained from BLOSS (Beijing, China). Mouse CTGF and Collagen I ELISA kits were provided by ABclonal Biotechnology. Other main reagents were supplied by Oriental Chemical Co. (Chongqing, China).

2.2. Preparation of ZnO nanoflowers on Ti surfaces

Firstly, the commercially pure titanium foils were cleaned under ultrasonication with acetone, ethanol, and distilled water for 15 min to remove impurities and contaminants. To prepare the precursor solution of ZnO, 2 g of zinc nitrate hexahydrate ($\text{Zn}(\text{NO}_3)_2 \cdot 6\text{H}_2\text{O}$) was dissolved in 200 mL distilled water and 6 mL of ammonia solution was added dropwise. Secondly, to obtain the ZnO seeding layer, the cleaned titanium foils were placed into an autoclave with 40 mL of ZnO precursor solution. Then the foils were hydrothermally treated at 70 °C for 16 h. Finally, after removing the excess reaction solution, to obtain a stable growth of ZnO nanoflowers on titanium foils, the samples were further annealed at 400 °C for 3 h. Then the resulting samples were thoroughly cleaned by distilled water and denoted as Ti-ZnO.

2.3. Synthesis of GelMA and HAMA

The synthesis of methacrylated gelatin (GelMA) was according to our previous works [36]. Briefly, 2 g of gelatin was dissolved in 100 mL of PBS (pH: 7.4) and stirred at 60 °C for 6 h. After the gelatin was completely dissolved, methacrylic anhydride (20%, v/v) was added to the above solution. After stirring and reacting for 6 h, the solution was diluted with warm PBS (40 °C) and dialyzed against distilled water for 7 days at 40 °C to remove excess methacrylic acid and other impurities. The obtained methacrylated gelatin solution was stored for further use.



Scheme 1. Schematic diagram of the self-adaptive strategy of this study.

The synthesis of methacrylated hyaluronic acid (HAMA) was according to another study [37]. Briefly, hyaluronic acid was diluted in distilled water (0.5 w/v, %). Then DMF was added to the solution with the ratio of DMF: H₂O = 2: 3. Then methacrylic anhydride was added dropwise into the above solution. The pH of the solution was adjusted to 9 by NaOH solution and reacting for 12 h. Finally, the solution was dialyzed against distilled water for 4 days and stored for further use.

2.4. Synthesis of GelMA-COOH and GelMA-PDA

To modify GelMA with catechol motifs, the carboxylation reaction of GelMA was firstly performed according to the study of Prof. Ali Khademhosseini's group [35]. Briefly, 1 g of GelMA was dissolved in 20 mL of PBS and stirred at 50 °C. Then 0.5 g of succinic anhydride was dissolved in 10 mL of DMSO, and this solution was added to the GelMA solution. 0.5 mL of triethylamine was added simultaneously. The mixture was continuously stirred overnight at 50 °C and diluted with PBS solution to stop the reaction. At last, the mixture was dialyzed against distilled water for 7 days and stored for further use.

Subsequently, the catechol motifs were conjugated with GelMA-COOH. Briefly, 1 g of GelMA-COOH was dissolved in 10 mL of MES buffer (pH: 5). Then 0.3 g of EDC, 0.3 g of NHS and 0.2 g of dopamine hydrochloride were added in turn, and the mixture was stirred for 12 h at room temperature. The resulting solution was dialyzed against 0.01 M HCl solution for 3 days and stored for further use.

2.5. Construction of hybrid hydrogel coatings on titanium

GelMA-PDA was dissolved in PBS solution to achieve a concentration of 10% (w/v). HAMA was also dissolved in PBS solution to achieve a concentration of 2.5% (w/v). Then the Ti-ZnO substrates were placed in

48-well plates. Next, different proportions of GelMA-PDA and HAMA solution were mixed as 4: 0, 3: 1, 1: 1 and 1: 3 (v/v). The total volume was 200 μL. Subsequently, the mixture was coated on Ti-ZnO substrates, and the photoinitiator Irgacure 2959 (0.3%, w/v) was added. Then the samples were exposed to 365 nm UV for 1 min. After being photocrosslinked, the samples were gently washed with PBS. Different groups of GelMA-PDA and HAMA hybrid hydrogel coatings on Ti-ZnO were denoted as Ti-ZnO/G, Ti-ZnO/G₃H₁, Ti-ZnO/G₁H₁, and Ti-ZnO/G₁H₃, respectively.

2.6. Sample characterizations

Firstly, the fabrication of ZnO nanoflowers on titanium substrates was characterized. The surface morphology and elements distribution were observed by a field emission scanning electron microscopy (SEM) (FEI Nova 400 Nano SEM, Phillips Co, Holland) and an energy-dispersive spectrometry (EDS, Zeiss AURIGA FIB, Germany). The surface roughness and surface crystalline phase were detected by atomic force microscopy (AFM, Dimension, Bruker, Germany) and X-ray diffraction (D/Max 2500 PC, Rigaku, Japan), respectively.

Secondly, the preparation of GelMA, GelMA-PDA, and HAMA hydrogels and the hybrid hydrogel coatings on titanium were characterized. The functional molecules of different hydrogels were detected by a nuclear magnetic resonance (NMR, AV500 MHz, Bruker, Swiss). The grafting ratios of GelMA-COOH and GelMA-PDA were also calculated.

2.7. The stability and enzyme-triggered degradation tests

The samples of Ti-ZnO/G, Ti-ZnO/G₃H₁, Ti-ZnO/G₁H₁ and Ti-ZnO/G₁H₃ were immersed in 500 μL of PBS, HAase (0.01, 0.05, 0.5 mg mL⁻¹)

and *S. aureus* solution (5×10^8 CFU) and incubated at 37 °C for 0, 2, 4, 6, 12, 24, 48, 72, 96, 120, 144 h. Thereafter, to calculate the mass remain of hydrogel coatings, the samples were lyophilized and weighted after being washed by PBS. The remaining mass was calculated based on the following formula:

$$RM = (M_t / M_0) \times 100\%$$

where RM means remaining mass. M_0 is the initial weights of samples. M_t is the weights of samples after being incubated for different time intervals. Three parallel samples of each group were measured.

In addition, after being incubated in PBS, HAase and *S. aureus* solution for 144 h, the samples were photographed to observe the stability of different samples. The samples after being immersed in PBS and HAase solution were also observed by SEM to study the degradation profile.

2.8. In vitro release of Zn ion

The Zn ion release of each group was studied. The samples were immersed in 5 mL of PBS and HAase solution (0.5 mg/mL) at 37 °C for 6, 24, 48, 72, 144 h and 28 days. The samples were also incubated with *S. aureus* solution (5×10^8 CFU) at 37 °C for 6, 24, 48, 72 and 144 h to observe the Zn ion release after the incubation with bacteria. The released Zn ion were detected by an inductively coupled plasma-atomic emission spectrometer (ICP-AES, Vista AX, Varian, USA) and the amount of each sample was calculated and analyzed. To ensure the accuracy, for each group, five same samples were incubated together to meet the requirements of ICP test.

2.9. Detection of ROS generation

The ROS generation of different samples was detected by a DCFH (2,7-Dichloro- fluorescein) probe method [38]. Briefly, 1 mmol L⁻¹ of DCFH-DA in methanol solution and 0.01 mol L⁻¹ NaOH solution was mixed (v: v = 1: 4). Then the mixture was stirred for 30 min in the dark, and the pH value was adjusted to 7.2. Subsequently, different samples were immersed in 1 mL of HAase solution (0.5 mg/mL). After different time intervals (0, 5, 10, 30 min and 2, 6, 24, 96, 144 h), 500 μL of the mixture was added to the supernatant of each sample. Finally, the generated ROS would oxidize DCFH to form DCF with fluorescent. Therefore, the yield of DCF of different samples was measured by a fluorophotometer (excitation wavelength: 485 nm, emission wavelength: 525 nm).

2.10. In vitro antibacterial tests

2.10.1. Bacteria culture

The *S. aureus* (ATCC29213) and *E. coli* (ATCC25922) were selected as the representative Gram-positive bacteria and Gram-negative bacteria, respectively. They were cultured in MHB medium and the bacteria concentrations were reflected by optical density (OD) at $\lambda = 600$ nm.

2.10.2. Short-term bacteria survival rates

The bacteria survival rate at the early phase was tested by the plate counting method. The samples were placed in a 24-well plate and 1 mL of *S. aureus* and *E. coli* suspension (1×10^6 CFU/mL) were added, respectively. After being incubated at 37 °C for 6 and 24 h, the medium was discarded, and the samples were rinsed with PBS three times. Then the samples were immersed with 1 mL of PBS and ultrasonically detaching for 10 min. The resulting bacteria suspension was diluted 10000-fold and 10 μL of them was distributed evenly onto agar plates. Then the agar plates were incubated at 37 °C for 20 h. The numbers of colony-forming units (CFUs) of each group were counted, and the bacteria survival rate was calculated based on the following formula:

$$\text{Bacteria survival rate (\%)} = \text{CFU of experimental groups} / \text{CFU of}$$

control $\times 100\%$

The average CFU was obtained from six independent experiments.

Subsequently, the adhesion of *S. aureus* and *E. coli* onto different samples at the early phase was observed by fluorescence staining. Briefly, 1 mL of *S. aureus* and *E. coli* suspension (1×10^6 CFU/mL) were incubated with different samples at 37 °C for 24 h. Afterward, the samples were washed by PBS three times and fixed with glutaraldehyde solution (4 wt%) at 4 °C overnight. The samples were then stained by Hoechst 33258 for 10 min and imaged by a confocal laser scanning microscopy (CLSM, TCS SP8, Leica, Germany).

2.10.3. Long-term antibacterial ability

Firstly, MTT assay was deployed to investigate the long-term antibacterial ability of different samples. In brief, 1 mL of *S. aureus* and *E. coli* suspension (1×10^6 CFU/mL) were cultured with different samples at 37 °C for 7 days. Then the suspension of different samples was collected and MTT dye was added according to the proportion of suspension: MTT dye = 9: 1 (v/v). Meanwhile, the samples were also gently washed by PBS and the culture medium, and MTT mixture were added to each well. All the samples were further incubated for 3 h. Next, the mixture was discarded, and 500 μL of dimethyl sulfoxide (DMSO) was added to dissolve the sediments. The samples were measured by using a spectrophotometric microplate reader (Bio-Rad 680) at 490 nm.

Secondly, the biofilm formation of different samples was studied by live/dead staining. Similarly, 1 mL of *S. aureus* suspension (1×10^6 CFU/mL) were cultured with different samples at 37 °C for 7 days. Mixed SYTO9 and PI dyes (Live/Dead BacLight bacterial viability kit, Invitrogen, USA) were used to stain the samples for 20 min. Alive and dead bacteria were stained green and red, respectively. Then the samples were observed and captured by CLSM.

Thirdly, the morphology change of *S. aureus* cultured on different samples for 7 days was studied. Briefly, 1 mL of *S. aureus* suspension (1×10^6 CFU/mL) were cultured with different samples at 37 °C for 7 days. Then the medium was removed and the samples were cleaned by PBS for three times. After that, the glutaraldehyde solution (4 wt%) was used to fix the samples for 30 min. Then the samples were dehydrated by a gradient ethanol solution (20%, 40%, 60%, 80%, and 100%) and lyophilized. Finally, after being sputter-coated with Au, the samples were observed and imaged by SEM.

2.10.4. Intracellular components leakage of *S. aureus*

Intracellular components leakage of *S. aureus* after being incubated with different groups was studied. Similarly, 1 mL of *S. aureus* suspension (1×10^6 CFU/mL) were cultured with different samples at 37 °C for 6 h, 24 h and 7 days, respectively. Then the OD₂₆₀ value of different groups was detected by an ultraviolet spectral photometer. Next, the total protein leakage after 7 days was measured by using a micro BCA Protein Assay Kit (Beyotime Biotechnology, China).

2.10.5. Exploration of antibacterial mechanism

To explore the antibacterial mechanism of ZnO, Vitamin C (10 mM) was employed as the ROS scavenger to counteract the potential effect of generated ROS from ZnO, and zinc ion standards was used to mimic the actual release amount of Zn²⁺ from Ti-ZnO/G, Ti-ZnO/G₃H₁, Ti-ZnO/G₁H₁, and Ti-ZnO/G₁H₃ groups after 7 days. Then 1 mL of *S. aureus* suspension (1×10^6 CFU/mL) were cultured with different samples at 37 °C for 7 days. The *S. aureus* viability was measured by MTT assay (the procedure was same with the above experiments).

2.11. In vitro cytocompatibility assessment

2.11.1. Cell culture

Fibroblast NIH/3T3 cell line (ATCC: CRL-1658) was kindly provided by Army Medical University (Chongqing, China). Cells were cultured with DMEM medium (high glucose) and supplemented with 10% of fetal bovine serum, streptomycin and penicillin. Besides, cells were

maintained at 37 °C in a constant humidity incubator with 5% CO₂. The culture medium was changed every two days.

2.11.2. Cell viability evaluation

The cell viability of NIH/3T3 cells cultured on different samples was tested by CCK-8 assay and live/dead staining. NIH/3T3 cells with a density of 2×10^4 cells/cm² were seeded on different samples and cultured for 1, 4 and 7 days. For the CCK-8 assay, the samples were slightly washed by PBS, and 10% of CCK-8/culture medium (v/v) was added into each well. After further incubating for 3 h, the supernatant of each well was collected and measured by a spectrophotometric microplate reader (Bio-Rad 680) at 450 nm. To evaluate the cell viability of NIH/3T3 cells on the samples that have been enzymatically degraded, different groups were incubated with *S. aureus* suspension (1×10^6 CFU/mL) for 144 h. Next, the *S. aureus* suspension was discarded and the samples were slightly washed by PBS for three times. Then the samples were treated by the ultraviolet radiation overnight and the NIH/3T3 cells were seeded on different samples for 2 days. The cell viability was also tested by the CCK-8 assay. For live/dead staining, after being washed by PBS, FDA/PI mixed solution (10 µg/mL) was added to each well, and the samples were incubated for 10 min. Then the samples were observed and imaged by CLSM.

2.11.3. ELISA assay

The contents of intracellular protein collagen I (COL-I) and connective tissue growth factor (CTGF) of NIH/3T3 cells was studied by ELISA assay. Briefly, 2×10^4 NIH/3T3 cells were seeded on different samples and cultured for 1, 4 and 7 days. Then the cells were washed by PBS and thoroughly lysed by 0.1% of Triton X-100. The content of total protein was determined by a micro BCA Protein Assay Kit (Beyotime Biotechnology, China) and the contents of COL-I and CTGF was determined by the ELISA kits.

2.11.4. Cytoimmunofluorescence staining

After being cultured on different samples, the expression of COL-I of NIH/3T3 cells was studied by cytoimmunofluorescence staining. Cells with a density of 2×10^4 were seeded and cultured for 7 days. Next, different samples were fixed by 4% of paraformaldehyde for 30 min, permeabilized by 0.2% of Triton X-100 for 5 min, and blocked by 1% BSA solution for 1 h. Then the samples were treated by primary antibody at 4 °C overnight. Subsequently, the samples were slightly washed to remove the primary antibody and coated with Alexa Fluor-488 secondary antibody for 30 min. The samples were then washed and further coated by Hoechst 33258 for another 10 min to stain cell nucleus. Finally, the samples were observed by CLSM.

2.11.5. Cell infiltration observation

The cells with a density of 1×10^4 cells/cm² were seeded on different samples for 7 days. The samples were then fixed by glutaraldehyde solution at 4 °C for 30 min and permeabilized by 0.2% of Triton X-100 solution for 5 min. Afterward, the samples were stained by Rhodamine-Phalloidin at 4 °C overnight. Finally, after being treated by Hoechst 33258 for 10 min to stain nuclei, the samples were observed and imaged by CLSM.

2.12. In vivo studies

2.12.1. Samples implantation and subcutaneous infection model

The animal surgery was operated according to the guidelines of the Institutional Animal Use Committee of China. The use of six-week-old male BALB/c mice for *in vivo* studies was approved by the Animal Ethics Committee of the Army Medical University (SYXK-PLA-20120031). The surgery was performed according to the former studies [39,40]: Briefly, all the BALB/c mice were randomly divided into three groups: Ti, Ti-ZnO, and Ti-ZnO/G₁H₃ (n = 4). Then they were anesthetized by 2 wt% of pentobarbital sodium solution (intraperitoneal

injection, 0.3 mL/kg). Next, the back of rats was shaved, and the dorsal wall skin was exposed. Two incisions were made (about 1.5 cm) along the sides of the spine to create a subcutaneous pocket model. Two samples in the same group were placed into the pocket for each mouse. At the same time, each pocket wound was injected with *S. aureus* (10^5 CFU). Then the subcutaneous tissues and skin were sutured, and the mice were cultured for 2, 7, 14 days, respectively.

2.12.2. In vivo anti-bacteria tests

To evaluate the anti-bacteria efficiency of different samples after implantation, the plate counting assay was used. Firstly, after culturing for 2 and 7 days, the mice were sacrificed and the tissues (contacting samples) were collected. The tissues were then cultured with 1 mL of sterile PBS and incubated for a further 12 h at 37 °C. After being diluted 50 times, 100 µL of the solution was used to add onto agar plates, and the colony number was counted after culturing for 24 h at 37 °C. The bacteria survival and inflammatory response of different tissues were also evaluated by Giemsa and H&E staining.

2.12.3. In vivo soft tissue compatibility tests

To evaluate the soft tissue compatibility of different samples, after culturing for 7 and 14 days, the mice were sacrificed and Ki67, TUNEL and Masson's trichrome staining was used respectively to reflect the cell proliferation, apoptosis and collagen deposition in the surrounding tissues.

2.12.4. Evaluation of the biosafety

To evaluate the biosafety of the samples, some important organs such as the heart, liver, spleen, lungs and kidneys of different groups were harvested and evaluated by H&E staining.

2.13. Statistical analysis

The immunofluorescence staining images in this study were analyzed by Image Pro-Plus 6.0. The data were presented as mean ± standard deviation. The statistical analysis were calculated with Origin Pro (version 8.5) by using Student's t-test and the confidence levels were set as: **p* < 0.05 and ***p* < 0.01.

3. Results and discussion

3.1. Characterization of ZnO nanoflowers on titanium

Fig. 1A explained the preparation method we used to fabricate ZnO nanoflowers on Ti surfaces. The ZnO nanoflowers were obtained by hydrothermal and annealing treatments. SEM images (Fig. 1B) suggested a clear nanoflower-like structure morphology was presented, and it was very stable since all the samples before SEM observation had been thoroughly ultrasonic cleaned. The SEM image of the nanoflower-like structure with a greater magnification (50000×) was shown in Figure S1. Compared with the direct deposition, this study's hydrothermal method made the ZnO structure more stable and the surface topography was comparably uniform [15]. EDS analysis in Fig. 1B illustrated that the chemical composition of the nanoflowers. Ti-ZnO samples exhibited clear signals of Zn and O, and the content of Ti decreased significantly. XRD test was further used to figure out the exact crystal phase of the nanoflowers. As shown in Fig. 1C, the Ti-ZnO group presented several typical peaks 31.8°, 34.4°, 36.3°, 62.9° and 77.0°, which corresponding to different crystal planes of ZnO (100), (002), (101), (103) and (202). Next, AFM analysis was used to reflect the surface roughness of pure titanium and Ti-ZnO, as shown in Figure S2, the Ra and Rq value of Ti was 27.4 and 36.8 nm. The Ra and Rq value of Ti-ZnO was 110 and 136 nm, respectively. The surface roughness of Ti-ZnO was significantly higher than pure titanium. The topological features, including roughness and surface morphology, may be useful to combat bacteria through the penetration of bacteria membrane or

inhibit the quick colonization. Several studies have reported the fabrication of ZnO structure by using the hydrothermal method [16,41,42]. These structures included nano-needles, nano-rods, or nano-flowers. These unique structures showed remarkable antibacterial activities due to the unique morphology. The higher surface area, special topology, and significant surface defects would combat pathogens by direct contact, the generation of ROS, and the release of Zn ions.

3.2. Characterization of hydrogels

The prepared GelMA, HAMA and the modification of catechol motifs to GelMA were characterized by NMR analysis. As shown in Fig. 1D, all the NMR spectra of GelMA, GelMA-COOH and GelMA-PDA exhibited peaks at 5.5 and 5.7 ppm corresponding to the $-C=CH_2$, which meant the successful methacrylation of gelatin. The peaks around 6.7 ppm of GelMA-PDA represented the hydrogen peak of phenolic hydroxyl, which demonstrated the successful addition of the catechol motifs to GelMA. The grafting ratios of GelMA-COOH and GelMA-PDA were also calculated based on the NMR results, which were 4.5% and 88.17%, respectively. Fig. 1E showed the NMR spectra of HAMA. Compared with pure hyaluronic acid, the spectrum of HAMA exhibited clear methacrylate peaks at 1.9 and 5.6 ppm, suggested the successful preparation of HAMA. The NMR peaks of GelMA, HAMA and GelMA-PDA was also consistent with the former studies [37,43].

3.3. Stability and enzyme-triggered degradation tests

Next, we tested the stability and enzyme-triggered degradation of the prepared GelMA-PDA/HAMA hybrid hydrogel on titanium and studied the influence of different proportions on the degradation rates. We prepared four groups: Ti-ZnO/G, Ti-ZnO/G₃H₁, Ti-ZnO/G₁H₁ and Ti-ZnO/G₁H₃, which represented different volume ratio of GelMA-PDA and HAMA. Firstly, the microscopic morphology change of the hydrogel coatings was observed by SEM. The four groups were cultured in PBS, HAase solution (0.5 mg mL⁻¹) and *S. aureus* suspension (5 × 10⁸ CFU/mL) for 144 h and imaged by SEM. As shown in Fig. 2A and Figure S4, after being incubated with PBS for 144 h, all the four groups still presented the typical lyophilized hydrogel morphology. The nanoflower-structure of ZnO was totally covered. When the groups were incubated with HAase solution and *S. aureus* suspension for 144 h, the Ti-ZnO/G group was still difficult to detect the ZnO structure beneath the coating. However, all the Ti-ZnO/G₃H₁, Ti-ZnO/G₁H₁ and Ti-ZnO/G₁H₃ presented clear cavities in the coating, and the ZnO structure was exposed. Next, the samples after being incubated with PBS (pH: 7.4), HAase solution (0.5 mg mL⁻¹) and *S. aureus* solution (5 × 10⁸ CFU) for 144 h was photographed (Figure S3). It was evident that all the hydrogel coatings were very stable on the titanium surfaces, even being incubated for 144 h. A tight adhesion was achieved, attributing to the catechol motifs. Moreover, the four groups in PBS showed unclear appearance change after 144 h of incubation. However, it was evident that Ti-ZnO/G₃H₁, Ti-ZnO/G₁H₁ and Ti-ZnO/G₁H₃ had less hydrogel residue than Ti-ZnO/G group after incubation with HAase or *S. aureus* solution.

To quantitatively study the enzyme-triggered degradation, different groups were incubated with PBS, HAase solution (0.01, 0.05, 0.5 mg mL⁻¹), and the remaining masses were calculated at different time points. Fig. 2B showed that compared with the Ti-ZnO/G group, all the groups of Ti-ZnO/G₃H₁, Ti-ZnO/G₁H₁ and Ti-ZnO/G₁H₃ exhibited various degree of accelerated degradation. After incubation of 144 h, the remaining mass of the groups of Ti-ZnO/G, Ti-ZnO/G₃H₁, Ti-ZnO/G₁H₁ and Ti-ZnO/G₁H₃ was 90.25%, 89.35%, 87.05% and 80.60%. The last group presented an obvious faster degradation compared with other groups. Fig. 2C–F exhibited the degradation profile of all the groups in different concentrations of HAase solution over 144 h. For the Ti-ZnO/G group, the degradation was slow and the concentrations of HAase also showed limited effect, as the remaining mass after 144 h was 95.71%, 95.01%, 94.65% and 94.35%. Then for the Ti-ZnO/G₃H₁ group, the

remaining mass was 95.60%, 83.35%, 82.49% and 81.05%. Compared with PBS (without HAase), the addition of different concentrations of HAase showed significant change about the degradation rates. Similarly, the remaining mass of Ti-ZnO/G₁H₁ group was 90.40%, 79.61%, 78.32% and 77.51%. And for Ti-ZnO/G₁H₃ group, it was 85.35%, 81.10%, 80.15% and 77.97%. The remaining mass of Ti-ZnO/G₁H₁ and Ti-ZnO/G₁H₃ group also exhibited a certain degree of decrease after being cultured in PBS. The potential explanation was: With the increase of the proportion of HAMA in the hydrogel coating, the adhesive property was slightly influenced as the catechol motifs were only modified on the chains of GelMA. These results indicated that although the adhesion of hydrogel coatings on the ZnO surface was stable, after incubation with HAase and *S. aureus* solution, the groups of Ti-ZnO/G₃H₁, Ti-ZnO/G₁H₁ and Ti-ZnO/G₁H₃ exhibited significantly accelerated degradation and the Ti-ZnO/G₁H₃ had the highest degradation rate.

The enzymatically-degradable property of hyaluronic acid has been widely reported before [44–46]. Compared with the enzyme secreted by Gram-negative bacteria, which is periplasmic, the HAase secreted by most Gram-positive bacteria is more important to play a role in degrading extracellular matrix and helping bacteria invade tissues. Various species of Gram-positive bacteria could secrete HAase including *Streptococcus*, *Staphylococcus*, *Peptostreptococcus*, *Propionibacterium*, and *Streptomyces*, etc [47]. In this study, our results showed a clear HAase-triggered degradation of hydrogel. Compared with PBS solution, different HAase and *S. aureus* solution concentrations exhibited clear effects of accelerating the degradation of hydrogel coatings (except Ti-ZnO/G group). In addition, the residue of the hydrogel coatings can still adhere to titanium.

3.4. Release profile of Zn ion

Because of the dose-dependent effect of Zn ion on both cells and bacteria, the release profile of Zn ion was measured. The samples of Ti-ZnO, Ti-ZnO/G₃H₁, Ti-ZnO/G₁H₁ and Ti-ZnO/G₁H₃ were incubated with PBS, HAase solution (0.5 mg/mL) and *S. aureus* solution (5 × 10⁸ CFU) for different durations. The results were shown in Fig. 2G and H and Figure S5. In the initial 144 h, Zn ion released from Ti-ZnO, Ti-ZnO/G, Ti-ZnO/G₃H₁, Ti-ZnO/G₁H₁ and Ti-ZnO/G₁H₃ in HAase solution was 6.63, 3.25, 3.20, 3.68, and 7.87 ppm, respectively. In PBS solution, they were 5.21, 2.25, 2.46, 2.43, and 2.50 ppm, respectively. After incubation for 28 days, the Zn ion released from Ti-ZnO, Ti-ZnO/G, Ti-ZnO/G₃H₁, Ti-ZnO/G₁H₁ and Ti-ZnO/G₁H₃ in HAase solution was 9.95, 7.27, 8.14, 8.39 and 9.32 ppm, respectively. In PBS solution, they were 6.56, 4.10, 5.16, 5.18 and 5.67 ppm, respectively. It was worth noting that in the initial 144 h, the release amount of the Ti-ZnO/G₁H₃ in HAase solution was higher than that of Ti-ZnO group. However, after 28 days, the total release amount of Ti-ZnO group was higher than the Ti-ZnO/G₁H₃ group. The potential explanation was: the detection of the amount of Zn ion in supernatant was largely influenced by the degradation of the hydrogel coatings. A sudden collapse may induce an instant acceleration of Zn ion release. Next, it was very clear that in PBS, the groups of Ti-ZnO/G, Ti-ZnO/G₃H₁, Ti-ZnO/G₁H₁ and Ti-ZnO/G₁H₃ showed a limited difference of Zn ion release. The Zn ion released from Ti-ZnO was much higher than the other four groups. Also, the release rates of these four groups in the first 14 days were all meager, which was crucial to improve cell viability. However, when being incubated with HAase solution, the Zn ion release of Ti-ZnO/G₁H₃ was much higher than Ti-ZnO/G, Ti-ZnO/G₃H₁ and Ti-ZnO/G₁H₁, which indicated that in HAase solution, the Zn ion release of Ti-ZnO/G₁H₃ can be noticeably accelerated. Moreover, the Zn ion release was further studied by incubating samples in *S. aureus* solution. The results (Figure S5) showed that the groups of Ti-ZnO, Ti-ZnO/G₁H₁ and Ti-ZnO/G₁H₃ showed a similar trend. The total release amounts of Ti-ZnO, Ti-ZnO/G₁H₁ and Ti-ZnO/G₁H₃ group after 144 h were 6.27, 6.07 and 5.94 ppm, respectively. The Zn ion released from Ti-ZnO/G₃H₁ and Ti-ZnO/G groups were 4.92 and 4.13 ppm. Compared with the Ti-ZnO/G group, the Zn ion release in the

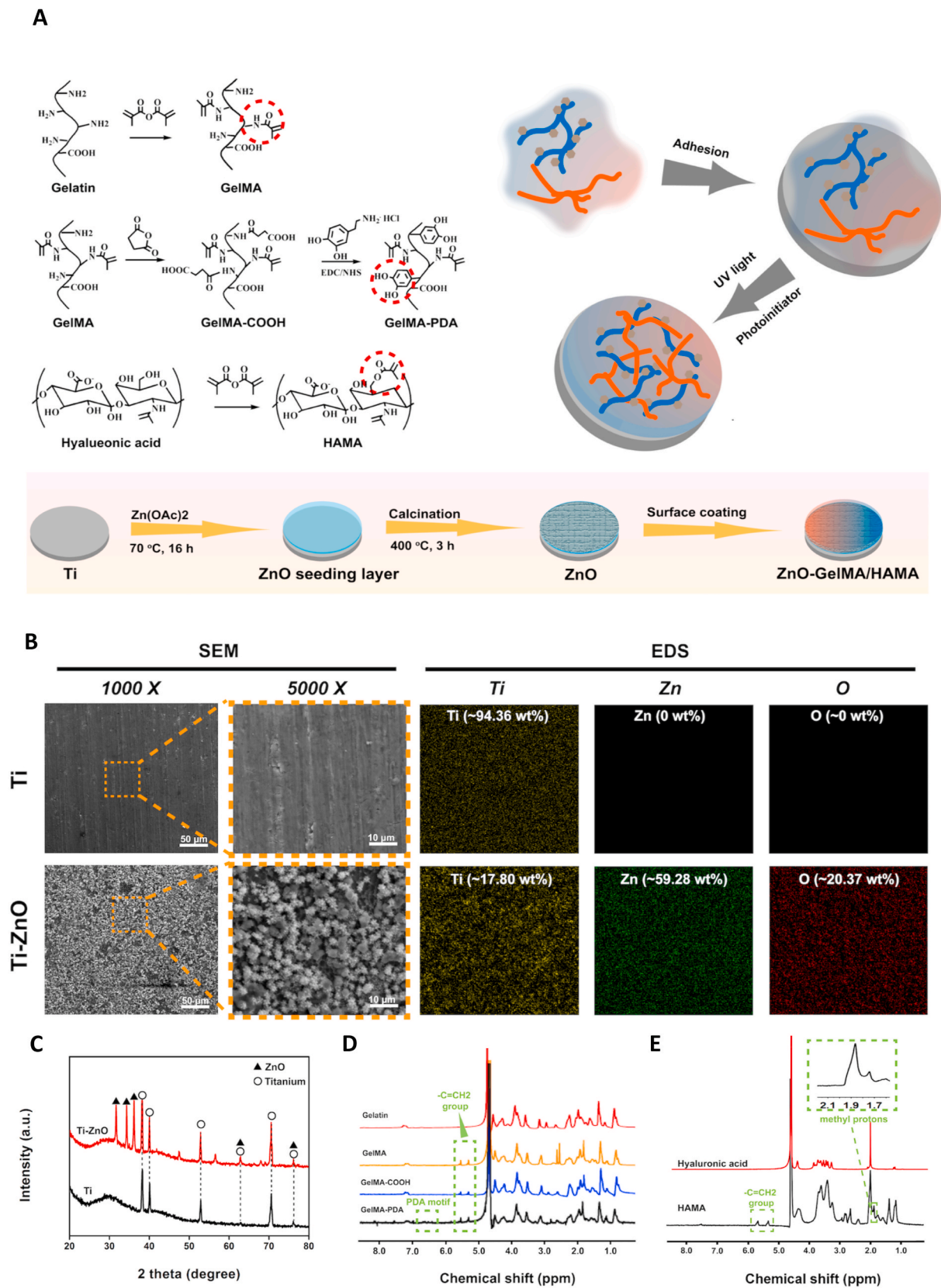


Fig. 1. (A) Schematic illustration of hydrogel synthesis, ZnO fabrication, and sample preparation. (B) Representative SEM images and EDS analysis of Ti and Ti-ZnO groups. (C) XRD test of Ti and Ti-ZnO groups. (D) and (E) NMR analysis of different hydrogel precursors.

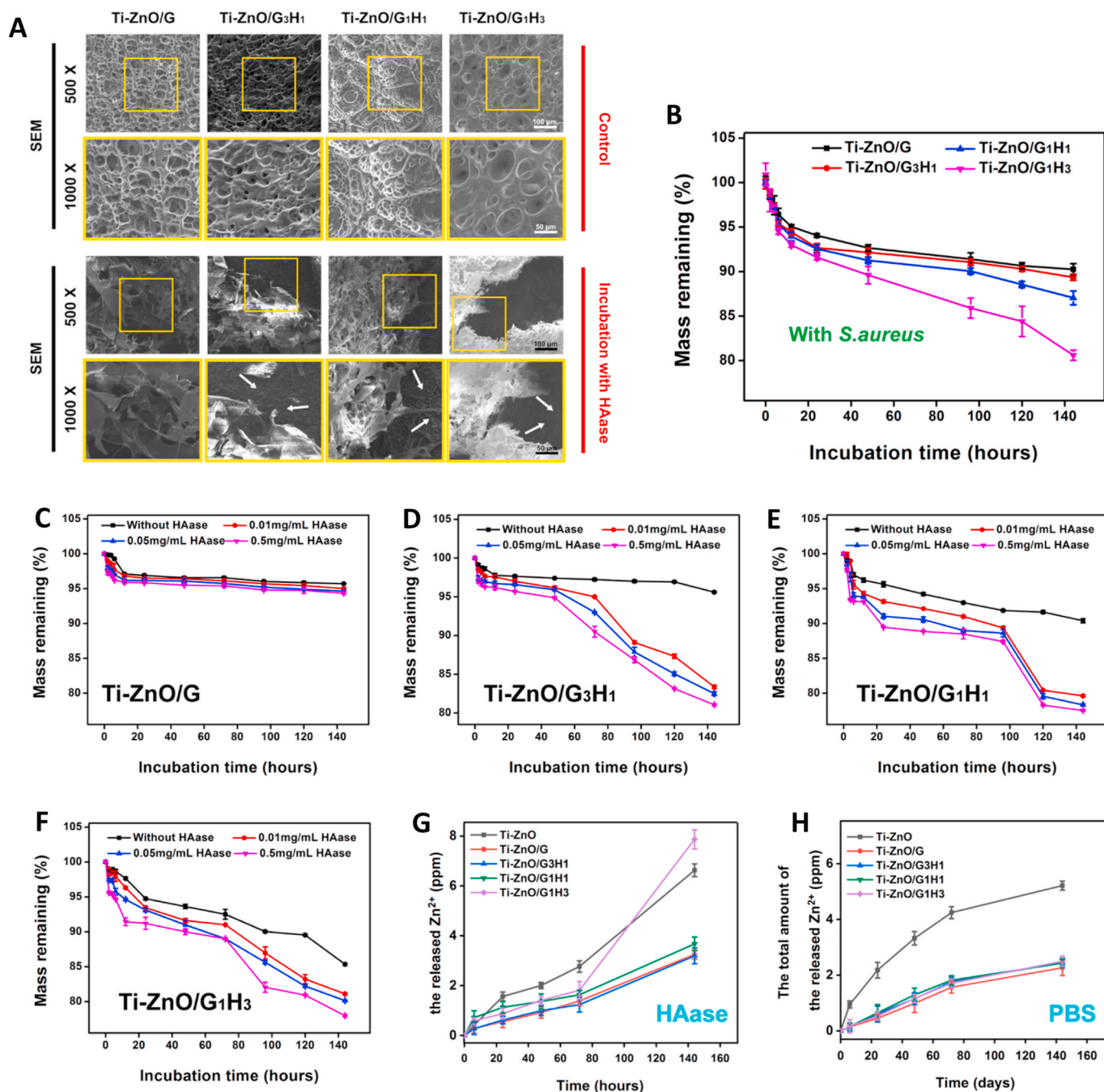


Fig. 2. (A) Representative SEM images of different groups after incubation with PBS and HAase solution for 144 h. (B) Degradation test of different groups when incubating with *S. aureus*. (C)–(F) Degradation test of different groups when incubating with PBS and different concentrations of HAase solution. (G) and (H) Zn ion release detection of different groups when incubating with PBS and HAase solution.

groups with the introduction of HAMA was accelerated.

3.5. ROS generation in vitro

The generation of ROS is one of the most important antibacterial mechanisms of ZnO structure [48]. The higher surface area and significant surface defects-induced oxygen vacancy would induce the generation of ROS. Therefore, the *in vitro* ROS generation of different samples was detected. As shown in Figure S7, it was clear that except for the Ti and Ti-ZnO/G groups, all the other groups showed obvious ROS generation, as the photoluminescence intensity at 525 nm had clear peaks, especially after 96 and 144 h. The introduction of GelMA hydrogel clearly inhibit the release of ROS into the supernatant. With the increase

of the proportion of HAMA, because of the accelerated degradation of the hydrogel coatings, more released ROS could be detected in the supernatant, especially after 96 and 144 h. Therefore, the release profile of ROS was similar with that of Zn²⁺.

3.6. Antibacterial activity in vitro

Several *in vitro* antibacterial tests were performed to understand the antibacterial efficiency. Firstly, the short term antibacterial ability was studied. From the quantitative results shown in Fig. 3A–C, the Ti-ZnO sample exhibited significant efficiency against *E. coli* and *S. aureus* after being incubated for 6 and 24 h. For *E. coli*, the corresponding survival rates could reduce to 12.73% and 19.00%, compared with the

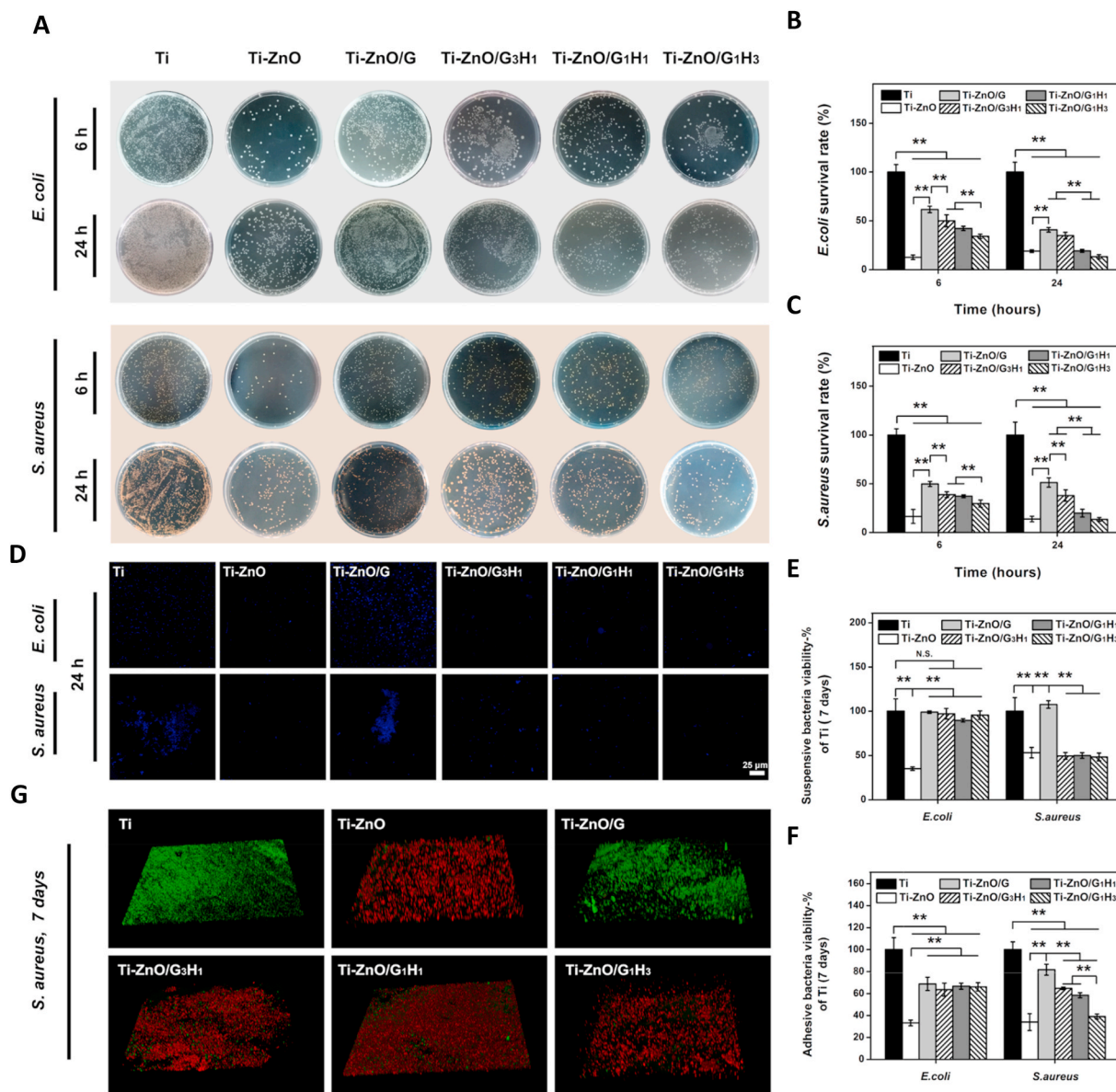


Fig. 3. (A) Representative plates of *E. coli* and *S. aureus* colonies after incubating with different groups for 6 and 24 h. (B) and (C) The corresponding quantitative statistics of the survival rates of *E. coli* and *S. aureus*. (D) Representative fluorescence images of *E. coli* and *S. aureus* colonies after incubating with different groups for 24 h. The bacteria were stained by Hoechst 33258 (blue). (E) and (F) The viability of suspensive and adhesive *E. coli* and *S. aureus* after incubating with different groups for 7 days. (G) The live/dead staining of *S. aureus* after incubating with different groups for 7 days (* $p < 0.05$, ** $p < 0.01$).

Ti group. For *S. aureus*, the survival rates could reduce to 16.46% and 13.20%. These results meant the ZnO nanoflowers on titanium surface had obviously antibacterial ability. However, after introducing different hydrogel coatings, the survival rates of *E. coli* and *S. aureus* of different groups slightly increased. For the Ti-ZnO/G group, the survival rates of *E. coli* were 61.60% and 40.79%, the survival rates of *S. aureus* were 49.69% and 51.29%, respectively. Obviously, for a short-term incubation, the GelMA coating largely influenced the antibacterial ability of ZnO. Similarly, for the Ti-ZnO/G₃H₁ group, the survival rates of *E. coli* were 49.92% and 34.89%, the survival rates of *S. aureus* were 38.82% and 37.89%. However, the groups of Ti-ZnO/G₁H₁ and Ti-ZnO/G₁H₃ can restore a good antibacterial ability, especially after 24 h of incubation. For the Ti-ZnO/G₁H₁ group, the survival rates of *E. coli* were 42.19% and 19.30%, the survival rates of *S. aureus* were 37.22% and 19.91%, respectively. For the Ti-ZnO/G₁H₃ group, the survival rates of *E. coli* were 34.15% and 13.32%, the survival rates of *S. aureus* were 29.62% and 13.46%. Immunofluorescence staining was further used to

study the bacteria adhesion at the initial phase. As shown in Fig. 3D, after being cultured for 24 h, it was very clear that large number of *E. coli* and *S. aureus* could be found in the groups of Ti and Ti-ZnO/G. In contrast, fewer colonies were presented in Ti-ZnO/G₃H₁, Ti-ZnO/G₁H₁ and Ti-ZnO/G₁H₃ groups. This tendency was also consistent with the quantitative results. The above results indicated that for a short-term incubation (within 24 h), the Ti-ZnO group exhibited obvious antibacterial ability against *E. coli* and *S. aureus*. The antibacterial ability of Ti-ZnO/G group was largely limited but with the increase of the proportion of HAMA, the antibacterial ability was enhanced. However, the results of the short-term incubation were difficult to know whether the reduced bacteria colonies were attributed to the direct bacteria killing or the anti-adhesive ability of hyaluronic acid. Therefore, the long-term antibacterial tests after bacteria were fully colonized were necessary.

Subsequently, the long-term antibacterial tests were further performed. *E. coli* and *S. aureus* were cultured for 7 days on different samples. Firstly, MTT assay was deployed to learn bacteria viability after 7

days. In addition, to explore whether *E. coli* and *S. aureus* can be directly killed, the bacteria viability both in medium and on the surface of the samples was tested (Fig. 3E & F). It was worth noting that after 7 days of incubation, only the Ti-ZnO group showed significant antibacterial ability against the *E. coli* in the medium. The *E. coli* viability in Ti-ZnO/G, Ti-ZnO/G₃H₁, Ti-ZnO/G₁H₁ and Ti-ZnO/G₁H₃ had no statistical difference with the Ti Group. However, for *S. aureus*, Ti-ZnO/G₃H₁, Ti-ZnO/G₁H₁ and Ti-ZnO/G₁H₃ groups showed comparable antibacterial ability with the Ti-ZnO group. The Ti-ZnO/G group had no distinct antibacterial ability against *S. aureus*. Next, the bacteria viability on the sample surfaces was tested. Although Ti-ZnO/G, Ti-ZnO/G₃H₁, Ti-ZnO/G₁H₁ and Ti-ZnO/G₁H₃ groups showed a significant decrease of *E. coli* viability compared with the Ti group, they were still much higher than that of the Ti-ZnO group. For *S. aureus*, all the Ti-ZnO/G, Ti-ZnO/G₃H₁ and Ti-ZnO/G₁H₁ groups presented reduced viability compared with the Ti group, but only the Ti-ZnO/G₁H₃ group had the comparable antibacterial ability with the Ti-ZnO group. Furthermore, live/dead staining was also used to observe bacteria viability visually. Different samples were incubated with *S. aureus* over 7 days and stained by live/dead BacLight bacterial viability kit. Then they were imaged by CLSM. As shown in Fig. 3G, the result was consistent with MTT assay, Ti-ZnO/G₁H₃ group showed similar antibacterial ability with Ti-ZnO. Ti-ZnO/G

group showed limited antibacterial ability. The groups of Ti-ZnO/G₃H₁ and Ti-ZnO/G₁H₁ could also reduce *S. aureus* viability, but some alive bacteria can still be observed (green regions). These results explained that after a long-term incubation, the antibacterial ability of Ti-ZnO/G, Ti-ZnO/G₃H₁, Ti-ZnO/G₁H₁ and Ti-ZnO/G₁H₃ groups against *E. coli* was limited. However, they had better antibacterial ability against *S. aureus*, and the Ti-ZnO/G₁H₃ group had the most remarkable efficiency.

Next, we used SEM to observe the morphology of samples and *S. aureus* after the 7 days of incubation. As shown in Fig. 4A, for the Ti group, the bacteria colonies were obvious. For the Ti-ZnO group, the ZnO structure was presented, and the alive bacteria had almost disappeared. We can find the hydrogel coating of the Ti-ZnO/G group was still very intact, and the adhered *S. aureus* was also very clear. For the groups of Ti-ZnO/G₃H₁, Ti-ZnO/G₁H₁ and Ti-ZnO/G₁H₃, the hydrogel residue was showed and the morphology of *S. aureus* obviously changed. The bacteria membrane became wrinkled and incomplete, which indicated the abnormal viability of *S. aureus*.

At last, the leakage of intracellular components of *S. aureus* was studied. *S. aureus* was incubated with different samples for 6 h, 24 h and 7 days, respectively. OD₂₆₀ value represented the leakage of nucleic acid. As shown in Fig. 4B, after 6 h of incubation, the OD₂₆₀ value of each group did not show any statistical difference. However, after 24 h and 7

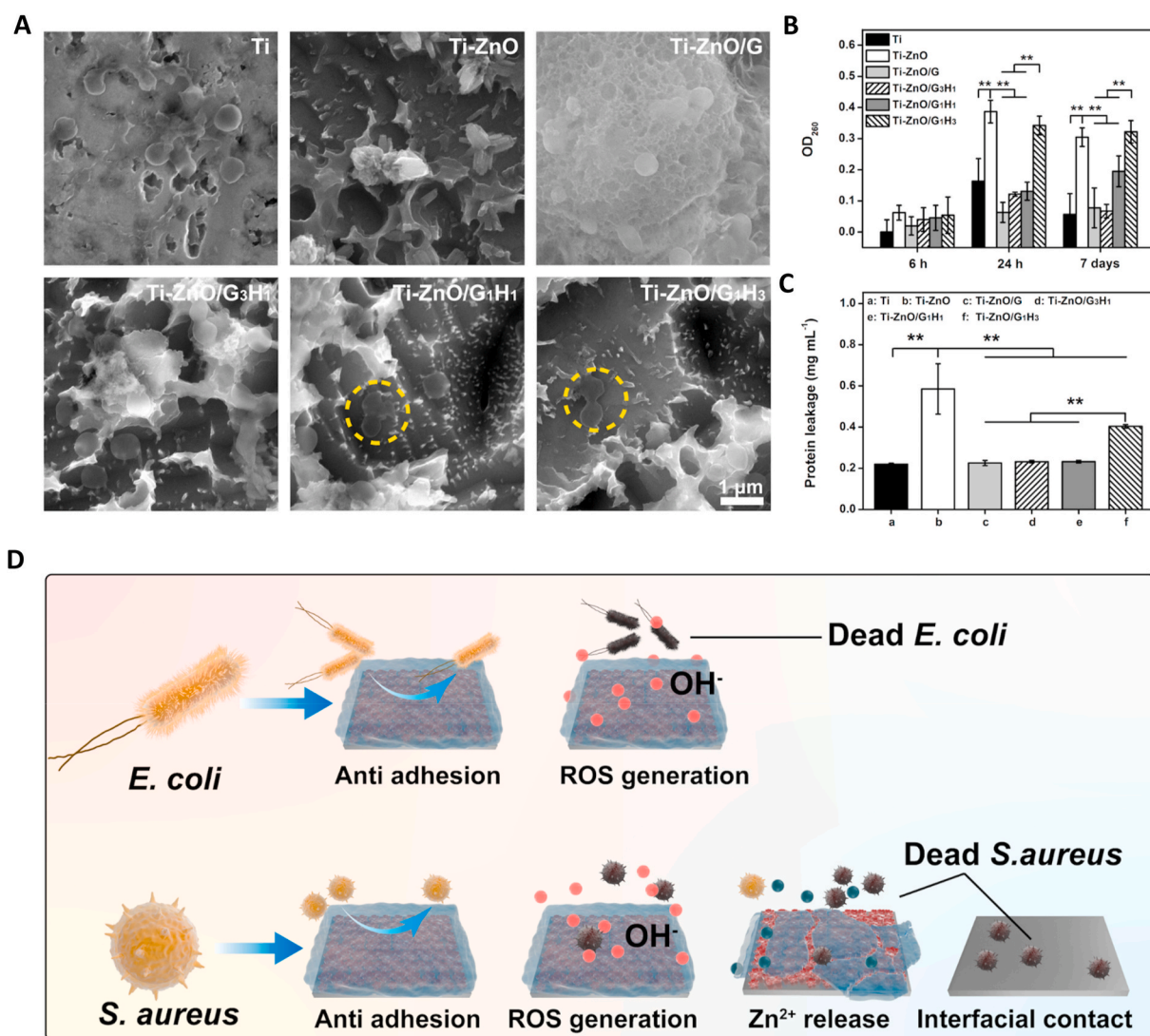


Fig. 4. (A) Representative SEM images of *S. aureus* after incubating with different groups for 7 days. Yellow circle represented the dead bacteria. (B) OD₂₆₀ value of *S. aureus* after incubating with different groups for 6 h, 24 h and 7 days. (C) Protein leakage test of *S. aureus* after incubating with different groups for 7 days. (D) The antibacterial mechanism illustration (**p* < 0.05, ***p* < 0.01).

days, the groups of Ti-ZnO and Ti-ZnO/G₁H₃ presented extremely high OD₂₆₀ value and the group of Ti-ZnO/G₁H₁ also exhibited significantly higher OD₂₆₀ value than Ti, Ti-ZnO/G and Ti-ZnO/G₃H₁ groups. Subsequently, the protein leakage after 7 days of incubation was also tested. As shown in Fig. 4C, similar to the result of OD₂₆₀ value test, the groups of Ti-ZnO and Ti-ZnO/G₁H₃ had a significantly higher amount than other groups.

In this study, firstly, Ti-ZnO exhibited efficient antibacterial ability against both *E. coli* and *S. aureus*. After the introduction of hydrogel coatings, the samples could maintain a certain degree of antibacterial ability, and it was enhanced along with the increased proportion of HAMA, which may be attributed to the anti-adhesive ability of hyaluronic acid. However, after a long-term of incubation, the antibacterial ability against *S. aureus* was much better than that of *E. coli* and the groups of Ti-ZnO/G₁H₃ had the best efficiency. *S. aureus* can secrete HAase and the degradation of the hydrogel coating was accelerated. The Zn ion release could be promoted and more surface regions of ZnO was exposed to direct contact with bacteria (Fig. 4D). Therefore, the Ti-ZnO/G₁H₃ group showed a remarkable ability against *S. aureus*.

The antibacterial mechanism of ZnO was complicated. It was certain

that the fabrication of nano/micro scale of ZnO could bring several unique properties to present antibacterial activity [49,50]. The higher surface area and significant surface defects-induced oxygen vacancy would enhance the release of Zn ions and the generation of ROS. In addition, the special shape of ZnO could also be useful to penetrate bacteria membrane or inhibit the colonization. To explore the antibacterial mechanism of ZnO, *S. aureus* was incubated with Ti, Ti-ZnO, Ti-ZnO + Vitamin C, and different dosages of zinc ion standards which in accordance with the actual release amount of Zn²⁺ from Ti-ZnO/G, Ti-ZnO/G₃H₁, Ti-ZnO/G₁H₁, and Ti-ZnO/G₁H₃ groups. Vitamin C was employed as the ROS scavenger to counteract the potential effect of ROS. As shown in Figure S8, after the addition of Vitamin C, the antibacterial ability of Ti-ZnO was impaired a little, which indicated that the generated ROS had antibacterial effect. In addition, the actual Zn²⁺ release amount of Ti-ZnO/G₁H₃ group also showed better antibacterial effect, compared with Ti-ZnO/G, Ti-ZnO/G₃H₁, and Ti-ZnO/G₁H₁ groups. This result helped us better understand the potential antibacterial mechanism of ZnO. Because the Zn²⁺ release amount of Ti-ZnO/G₁H₃ group showed comparable antibacterial effect with Ti-ZnO group, it was reasonable to conclude that Zn²⁺ had a predominant

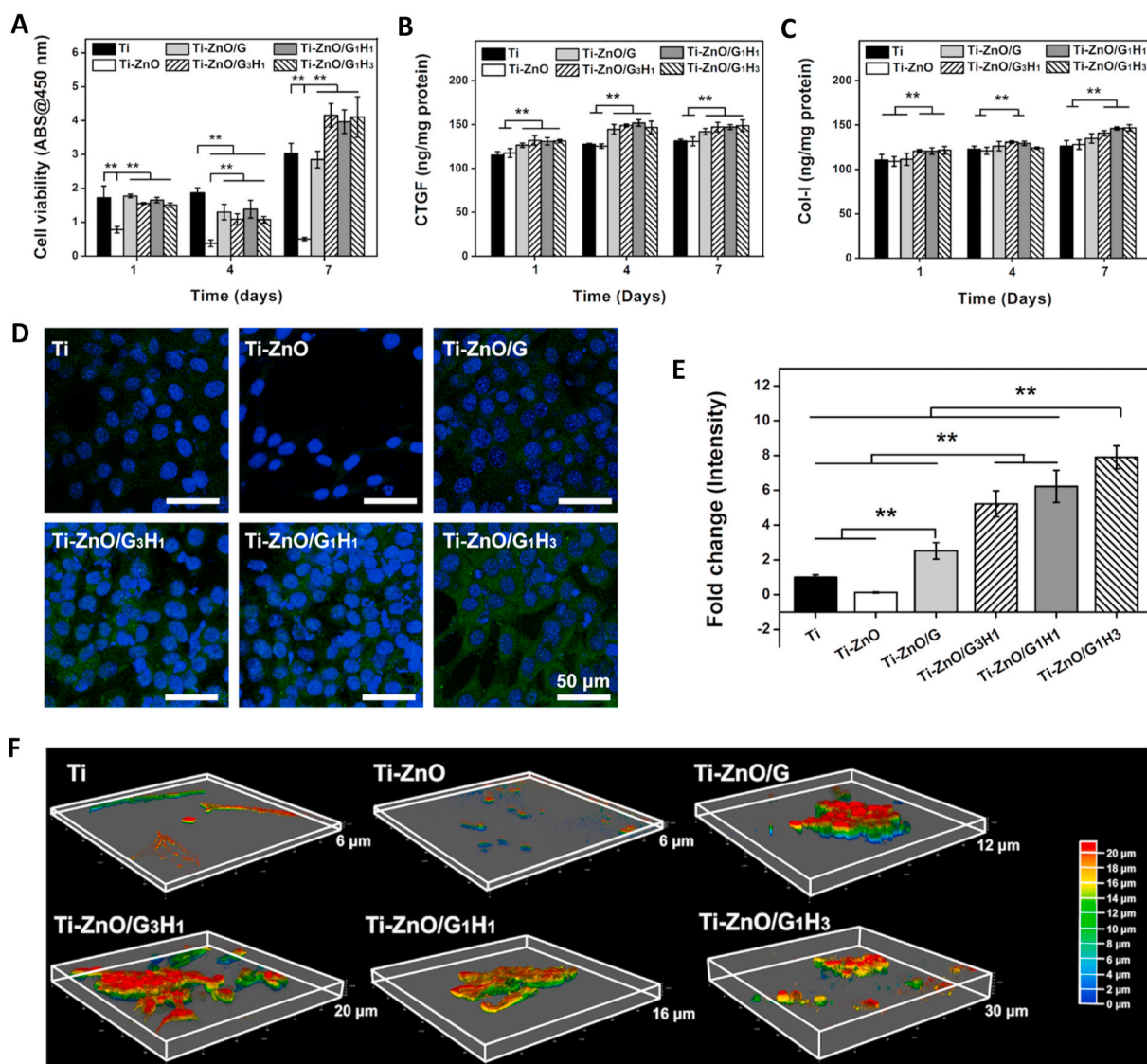


Fig. 5. (A) Cell viability test of NIH/3T3 after incubating with different groups for 1, 4 and 7 days. (B) CTGF expression of NIH/3T3 after incubating with different groups for 1, 4 and 7 days. (C) COL-I expression of NIH/3T3 after incubating with different groups for 1, 4 and 7 days. (D) Representative fluorescence images of COL-I expression after incubating with different groups for 7 days. (E) The corresponding quantitative statistics of COL-I expression. (F) 3D cell morphology observation after incubating with different groups for 7 days (**p* < 0.05, ***p* < 0.01).

antibacterial role. Moreover, ROS was also helpful to combat bacteria.

3.7. Fibroblast responses in vitro

Cyto-compatibility is important for the development of implantable biomaterials. Fibroblasts undertake heavy roles in soft-tissue growth. Accordingly, we focused on the influence of our samples on fibroblast responses in the normal condition (with no bacterial contamination). Firstly, the viability of NIH/3T3 cells cultured on different samples was tested by CCK-8 assay. As shown in Fig. 5A, the Ti-ZnO group showed the obvious cytotoxicity. After the addition of hydrogel coatings, the cell viability could be largely improved. Especially after 7 days, the cell viability of Ti-ZnO/G₃H₁, Ti-ZnO/G₁H₁ and Ti-ZnO/G₁H₃ groups were even significantly higher than that of the Ti group. It was worth noting that except the Ti group, the cell viability of other groups after 4 days exhibited a slight dropping compared with that of 1 day. Exactly, ZnO had a significant negative influence on the cell viability of NIH/3T3 cells and this negative effect was not fully reflected after 1 day. However, the cell proliferation was greatly influenced as the cell viability after 4 days was even lower than that of 1 day. This negative effect could be totally covered even after 7 days as the cell viability of all groups showed a clear increase. The cell viability was further directly observed by live/dead staining. As shown in Figure. S9, the cells in the Ti-ZnO group were obviously less than other groups and more dead cells were observed. The other five groups had no clear difference. Although a few dead cells can be found, the alive cells were still dominated and presented typical spindle morphology, consistent with the CCK-8 assay.

Zinc is one of the most abundant trace elements in soft tissues and undertakes pivotal physiological roles to regulate cell behaviors. According to the previous report [51,52], zinc could improve fibroblast proliferation and participate in various protein synthesis processes. Zinc is the key component of several functional molecules such as matrix metalloproteinases, integrins and zinc finger related factors [53]. These functional molecules are widely involved in physiological behaviors and therefore, an appropriate concentration of zinc release may be beneficial for soft tissue regeneration. Therefore, we tested several fibroblast behaviors after being incubated with different samples. First of all, we focused on the expression of two important factors: CTGF and COL I. CTGF is an important indicator of fibroblast functions (being activated and participated in wound repair) and COL I secretion is one of the main roles of fibroblasts. According to ELISA results (Fig. 5B and C), for the intracellular amount of CTGF, all the CTGF amounts of the Ti-ZnO/G, Ti-ZnO/G₃H₁, Ti-ZnO/G₁H₁ and Ti-ZnO/G₁H₃ were higher than the Ti and Ti-ZnO groups after 1, 4, and 7 days, which indicated a clear tendency that after the addition of hydrogel coatings, the expression of CTGF was improved. Then for COL I, after 1 day, the groups of Ti-ZnO/G₃H₁, Ti-ZnO/G₁H₁ and Ti-ZnO/G₁H₃ had the higher amounts than the Ti, Ti-ZnO and Ti-ZnO/G group. After 4 days, only the groups of Ti-ZnO/G₃H₁, Ti-ZnO/G₁H₁ had the higher amounts than the Ti and Ti-ZnO group. Then after 7 days, the COL I amount of the groups of Ti-ZnO/G₃H₁, Ti-ZnO/G₁H₁ and Ti-ZnO/G₁H₃ were higher than that of Ti and Ti-ZnO groups. These results indicated that the intracellular amounts of CTGF and COL I were increased after the introduction of hydrogel coatings. It was worth noting that although the Ti-ZnO group presented a low cell viability, the expression of CTGF and COL I was not significantly influenced. The potential explanation was the total numbers of CTGF and COL I had been normalized by the amounts of total protein. Therefore, although the cell viability of the Ti-ZnO group was low, the expression of CTGF and COL I still showed comparable results with other groups.

The COL-I expression of different groups was also observed by immunofluorescence staining. As shown in Fig. 5D, the green region in images represented the COL-I. According to the quantitative results (Fig. 5E), The group of Ti-ZnO/G₁H₃ had the highest amount of COL I, which was consistent with the result of the ELISA study.

At last, cell migration and infiltration were also significant for soft

tissue regeneration. The hydrogel coating provides a huge advantage to titanium in that it allows fibroblast ingrowth. Therefore, we further explored the cytoskeleton spread and fibroblast ingrowth after being seeded on different samples for 7 days. The cytoskeleton was stained by Rhodamine-Phalloidin, and the Z-stack images were captured by CLSM and remodeled in a 3D volumetric manner. As shown in Fig. 5F, for the Ti group, the cells presented the typical 2D spread profile, with limited ingrowth. For the Ti-ZnO group, because of the toxicity, the cytoskeleton was hard to be observed. For the groups of Ti-ZnO/G, Ti-ZnO/G₃H₁, Ti-ZnO/G₁H₁ and Ti-ZnO/G₁H₃, the cells showed clear 3D morphology and the ingrowth depth could achieve 12, 20, 16 and 30 μm, respectively. The increase proportion of HAMA in hydrogel coating can not only accelerate its degradation, but also improve cell spread in a 3D manner.

In the normal condition, hydrogel coatings can effectively alleviate the toxicity of ZnO and improve cell viability by modulating the Zn ion release and reducing the direct contact between cells and ZnO. With the proportion of HAMA increases, the degradation was faster and the fibroblast ingrowth was promoted. In addition, the controlled Zn ion release may also be helpful for the expression of several key factors of fibroblasts.

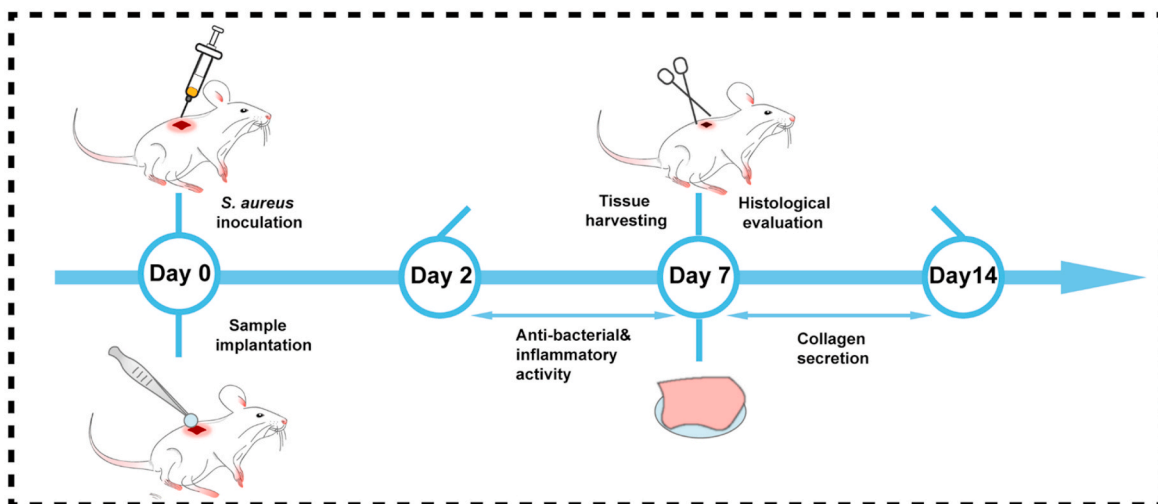
3.8. Fibroblast viability test after the samples incubating with *S. Aureus* solution

When *S. aureus* exists, the hydrogel coating had a higher degradation rate, and Zn ion release was accelerated. More ZnO structure may also be exposed. Therefore, it is necessary to validate whether the samples after incubating with *S. aureus* are harmful to cell viability. Different samples were incubated with *S. aureus* for 144 h firstly, then after being totally sterilized, NIH/3T3 cells were seeded on the samples and cultured for another 2 days. The cell viability was tested by CCK-8 assay. As shown in Figure. S10, after 2 days, the Ti-ZnO group showed a significant lower value than other groups and all the groups of Ti-ZnO/G, Ti-ZnO/G₃H₁, Ti-ZnO/G₁H₁ and Ti-ZnO/G₁H₃ had no statistical difference with Ti group. Therefore, the samples after incubating with *S. aureus* had no obvious cytotoxicity. We speculated that for the Ti-ZnO/G₁H₃ group, most Zn ion and ROS had been already released in the first 7 days and the surface feature had limited adverse effects on fibroblasts. For the Ti-ZnO/G, Ti-ZnO/G₃H₁ and Ti-ZnO/G₁H₁ groups, the Zn ion release was slow, which also brought little adverse effects to fibroblasts.

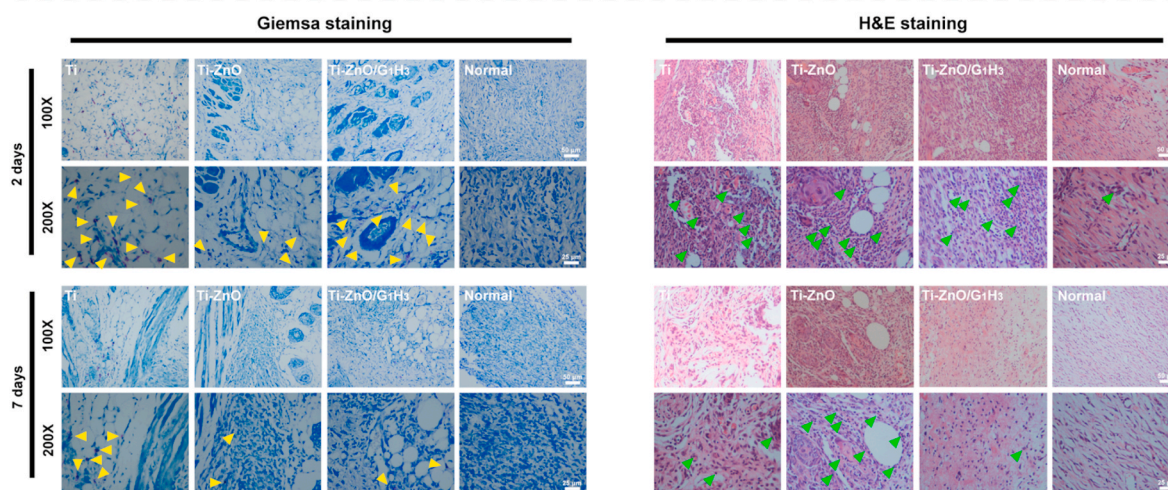
3.9. Infection inhibition efficiency in vivo

Bacterial infections can not only induce several diseases, but also destroy the natural organization of soft tissues and inhibit their regeneration. Biomaterials with the ability to inhibit bacterial infections and improving soft tissue compatibility hold great significance. Therefore, the infection inhibition efficiency and soft tissue compatibility were tested *in vivo* (Fig. 6A). *S. aureus* was inoculated subcutaneously and the groups of Ti, Ti-ZnO and Ti-ZnO/G₁H₃ were selected and placed. The infection condition was then evaluated by the plate counting method and histological staining. As shown in Fig. 6B, according to Giemsa staining, after two days, the stained bacteria (yellow arrows) can be observed in all three groups, but the amount of Ti-ZnO group was less than the other two groups. After 7 days, the stained bacteria in all groups had reduced but compared with Ti group, both the Ti-ZnO and Ti-ZnO/G₁H₃ groups had the less numbers, indicating an effective antibacterial ability. The result of H&E staining (Fig. 6B) was consistent with the Giemsa staining. The inflammatory infiltration was reflected by the numbers of neutrophils (green arrows). It was clear that after 2 days, a large number of neutrophils was presented in all three groups, which indicated the acute inflammatory response after bacterial infection and sample placement. However, after 7 days, the numbers of neutrophils in Ti and Ti-ZnO/G₁H₃ groups were significantly reduced. Massive stained neutrophils could still be observed in the group of Ti-ZnO. Therefore, the inflammatory response in the Ti-ZnO group was not well resolved even

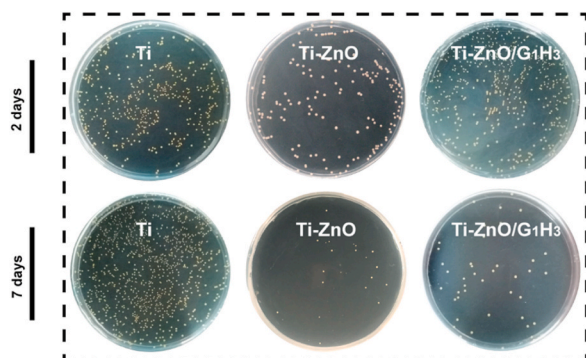
A



B



C



D

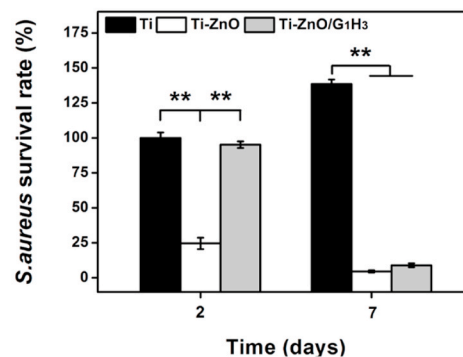


Fig. 6. (A) Schematic diagram of *in vivo* studies. (B) Giemsa and H&E staining of different groups after 2 and 7 days. Yellow arrows represented bacteria and green arrows represented the infiltrated neutrophils. (C) Representative plates of *S. aureus* colonies of different groups after 2 and 7 days. (D) Corresponding quantitative statistics of bacteria counts after 2 and 7 days (* $p < 0.05$, ** $p < 0.01$).

after 7 days.

Next, we quantitatively studied the antibacterial efficiency by culturing the *in vivo* *S. aureus* of different groups on agar plates. As shown in Fig. 6C and D, firstly, the Ti-ZnO group had a good antibacterial activity for both 2 and 7 days, as the *S. aureus* survival rates were 24.57% and 4.55%, respectively. In contrast, the groups of Ti and Ti-ZnO/G₁H₃ did not show clear antibacterial activity after 2 days. However, after 7 days, the Ti-ZnO/G₁H₃ group exhibited comparable antibacterial ability with the Ti-ZnO group, as the *S. aureus* survival rate was

8.95%. Therefore, it could be speculated that the Ti-ZnO/G₁H₃ group can effectively inhibit bacterial infection within 7 days. This result is reasonable as the hydrogel coating plays a really important role: possessing the antibacterial ability and curbing inflammatory response effectively.

3.10. Soft tissue compatibility in vivo

The *in vitro* experiments proved that the Ti-ZnO/G₁H₃ can not only

avoid the toxicity of ZnO, but also positively regulate the fibroblast responses. Therefore, in animal studies, we hoped that the samples could also be used to improve soft tissue compatibility. Firstly, the cell proliferation and apoptosis in the surrounding tissues was detected, as both inflammation and bacterial infection can influence cell growth and survival. The Ki67 staining was used to reflect cell proliferation (Fig. 7A). After 7 days, there was no obvious difference among all the groups, but after 14 days, the stained regions in Ti-ZnO/G₁H₃ group were much more than the other two experimental groups and the normal group, which meant the Ti-ZnO/G₁H₃ group had a better environment for cell growth and proliferation. Next, the TUNEL staining was also deployed to study cell apoptosis. After 7 days, compared with the normal group, all the experimental groups had many stained regions because of the bacterial infection and inflammatory response. However, after 14 days, Ti-ZnO/G₁H₃ group was better than Ti and Ti-ZnO groups. These results proved that compared with Ti and Ti-ZnO groups, the Ti-ZnO/G₁H₃ group was more beneficial for cell growth and proliferation in the surrounding tissues.

Subsequently, because bacterial infection and inflammation can largely destroy soft tissue structure and collagen organization, collagen deposition was further explored by Masson's trichrome staining. As shown in Fig. 7B, the collagen distribution of the Ti group was similar to the normal. However, the collagen deposition in the Ti-ZnO group was much lower than the other groups, which indicated an abnormal

condition of the tissue. The Ti-ZnO/G₁H₃ group had the best outcome, which reflected a good soft tissue compatibility.

4. Conclusions

In this study, a nanoflowers-like ZnO structure was constructed on titanium firstly, and an enzymatically-degradable coating tightly adhered on it. The fabricated sample exhibited a self-adaptive ability to possess both of remarkable antibacterial activity and soft tissue compatibility. Under bacterial infection, the hydrogel coating was degraded faster because of the HAase secreted by *S. aureus*. Then the exposed ZnO presented effective antibacterial ability. Under normal condition, the hydrogel coating was stable, and the toxicity of ZnO could be perfectly reduced. The curbed Zn ion release further positively regulated fibroblast behaviors. The *in vivo* studies also validated the remarkable bacterial infection inhibition, and soft tissue compatibility of the fabricated sample. The described enzymatically-degradable coating on titanium reported a feasible, effective and potential method to balance antibacterial activity and biosafety, which may have wider applications in the future.

CRediT authorship contribution statement

Jin Leng: Methodology, Data curation, Investigation, Visualization.

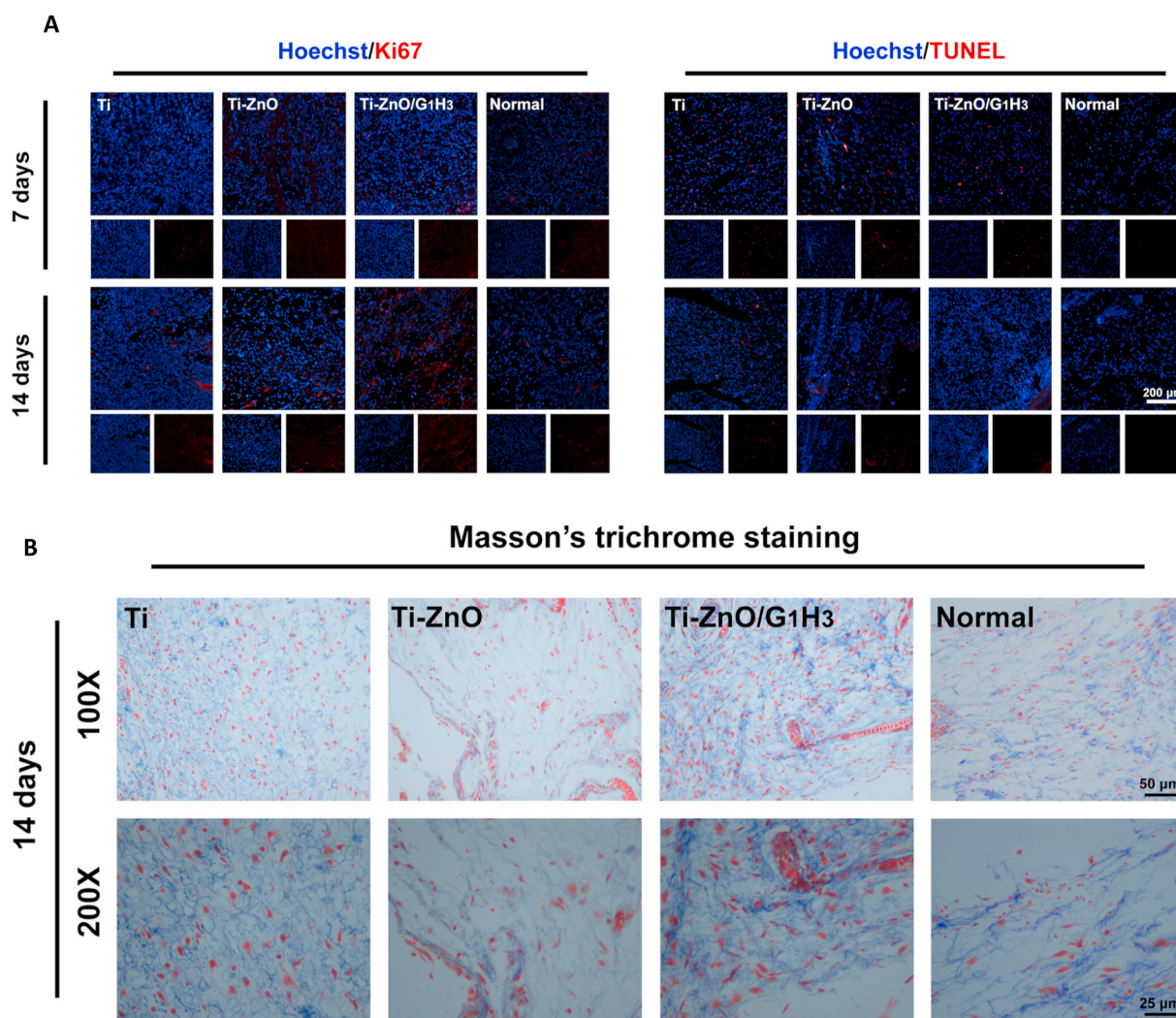


Fig. 7. (A) Representative fluorescence images of Ki-67 and TUNEL staining after 7 and 14 days. (B) Representative images of Masson's trichrome staining after 14 days.

Ye He: Conceptualization, Investigation, Data curation, Writing – original draft. **Zhang Yuan:** Investigation. **Bailong Tao:** Investigation. **Ke Li:** Investigation, Formal analysis. **Chuanchuan Lin:** Visualization. **Kun Xu:** Investigation. **Maowen Chen:** Investigation. **Liangliang Dai:** Investigation, Resources. **Xuemin Li:** Visualization. **Tony Jun Huang:** Validation. **Kaiyong Cai:** Conceptualization, Supervision, Writing – original draft.

Declaration of competing interest

The authors declare that they have no known competing financial interests or personal relationships that could have appeared to influence the work reported in this paper.

Acknowledgements

This work was financially supported by the National Natural Science Foundation of China (51825302, 21734002 & 52021004), and the State Key Project of Research and Development (Grant No. 2016YFC1100300 & 2017YFB0702603).

Appendix A. Supplementary data

Supplementary data to this article can be found online at <https://doi.org/10.1016/j.bioactmat.2021.05.001>.

References

- C.R. Arciola, D. Campoccia, L. Montanaro, Implant infections: adhesion, biofilm formation and immune evasion, *Nat. Rev. Microbiol.* 16 (2018) 397–409.
- C.R. Arciola, D. Campoccia, G.D. Ehrlich, L. Montanaro, Biofilm-based implant infections in orthopaedics, *Adv. Exp. Med. Biol.* 830 (2015) 29–46.
- B. Li, T.J. Webster, Bacteria antibiotic resistance: new challenges and opportunities for implant-associated orthopedic infections, *J. Orthop. Res.* 36 (2018) 22–32.
- X.K. Shen, Y.Y. Zhang, P.P. Ma, L. Sutrisno, Z. Luo, Y. Hu, Y.L. Yu, B.L. Tao, C.Q. Li, K.Y. Cai, Fabrication of magnesium/zinc-metal organic framework on titanium implants to inhibit bacterial infection and promote bone regeneration, *Biomaterials* 212 (2019) 1–16.
- M. Ribeiro, F.J. Monteiro, M.P. Ferraz, Infection of orthopedic implants with emphasis on bacterial adhesion process and techniques used in studying bacterial-material interactions, *Biomater* 2 (2012) 176–194.
- H. Katsutoshi, M. Shinya, Bacterial adhesion: from mechanism to control, *Biochem. Eng. J.* 48 (2010) 424–434.
- Q. Chen, G.A. Thouas, Metallic implant biomaterials, *Mater. Sci. Eng. R Rep.* 87 (2015) 1–57.
- S. Ye, C.A. Johnson Jr., J.R. Woolley, T.A. Snyder, L.J. Gamble, W.R. Wagner, Covalent surface modification of a titanium alloy with a phosphorylcholine-containing copolymer for reduced thrombogenicity in cardiovascular devices, *J. Biomed. Mater. Res. A* 1 (2009) 18–28.
- I. Narimatsu, I. Atsuta, Y. Ayukawa, W. Oshiro, N. Yasunami, A. Furuhashi, K. Koyano, Epithelial and connective tissue sealing around titanium implants with various typical surface finishes, *ACS Biomater. Sci. Eng.* 5 (2019) 4976–4984.
- Z. Yuan, B. Tao, Y. He, C. Mu, G. Liu, J. Zhang, Q. L. P. Liu, K. Cai, Remote eradication of biofilm on titanium implant via near-infrared light triggered photothermal/photodynamic therapy strategy, *Biomaterials* 223 (2019) 119479.
- B. Tao, W. Zhao, C. Lin, Z. Yuan, Y. He, L. Lu, M. Chen, Y. Ding, Y. Yang, Z. Xia, K. Cai, Surface modification of titanium implants by ZIF-8@Levo/LBL coating for T inhibition of bacterial-associated infection and enhancement of in vivo osseointegration, *Chem. Eng. J.* 390 (2020) 124621.
- Z. Yuan, B.L. Tao, Y. He, J. Liu, C.C. Lin, X.K. Shen, Y. Ding, Y.L. Yu, C.Y. Mu, P. Liu, K.Y. Cai, Biocompatible MoS₂/PDA-RGD coating on titanium implant with antibacterial property via intrinsic ROS-independent oxidative stress and NIR irradiation, *Biomaterials* 217 (2019) 119290.
- X. Chen, K. Cai, J. Fang, M. Lai, J. Li, Y. Hou, Z. Luo, Y. Hu, L. Tang, Dual action antibacterial TiO₂ nanotubes incorporated with silver nanoparticles and coated with a quaternary ammonium salt, *Surf. Coating. Technol.* 216 (2013) 158–165.
- I.A.J. van Hengel, N.E. Putra, M.W.A.M. Tierolf, M. Minneboo, A.C. Fluit, L. E. Fratila-Apachitei, I. Apachitei, A.A. Zadpoor, Biofunctionalization of selective laser melted porous titanium using silver and zinc nanoparticles to prevent infections by antibiotic-resistant bacteria, *Acta Biomater.* 107 (2020) 325–337.
- X. Wu, L. Yao, M.A. Al-Baadani, L. Ping, S. Wu, A.M. Al-Bishari, K. HiiRuYie, Z. Deng, J. Liu, X. Shen, Preparation of multifunctional drug sustained-release system by atomic T layer deposition of ZnO in mesoporous titania coating, *Ceram. Int.* 46 (2020) 9406–9414.
- J. Li, L. Tan, X. Liu, Z. Cui, X. Yang, K.W.K. Yeung, P.K. Chu, S. Wu, Balancing Bacteria–Osteoblast competition through selective physical puncture and biofunctionalization of ZnO/polydopamine/arginine-glycine-aspartic acid-cysteine nanorods, *ACS Nano* 11 (2017) 11250–11263.
- P. Sukanta, M. Sourav, M. Jayanta, In situ generation and deposition of ZnO nanoparticles on cotton surface to impart hydrophobicity: investigation of antibacterial activity, *Mater. Technol.* 33 (2018) 555–562.
- N. Garino, P. Sanvitale, B. Dumontel, M. Laurenti, M. Colilla, I. Izquierdo-Barba, V. Cauda, M. Vallet-Regi, Zinc oxide nanocrystals as a nanoantibiotic and osteoinductive agent, *RSC Adv.* 9 (2019) 11312–11321.
- P.E. Petrochenko, Q. Zhang, R. Bayati, S.A. Skoog, K.S. Phillips, G. Kumar, R. J. Narayan, P.L. Goering, Cytotoxic evaluation of nanostructured zinc oxide (ZnO) thin films and leachates, *Toxicol. Vitro* 28 (2014) 1144–1152.
- W. He, H.K. Kim, W.G. Wamer, D. Melka, J.H. Callahan, J.J. Yin, Photogenerated charge carriers and reactive oxygen species in ZnO/Au hybrid nanostructures with enhanced photocatalytic and antibacterial activity, *J. Am. Chem. Soc.* 136 (2014) 750–757.
- J. Lee, B.S. Kang, B. Hicks, C.T. Chancellor, B.H. Chu, H.T. Wang, B.G. Keselowsky, F. Ren, T.P. Lele, The control of cell adhesion and viability by zinc oxide nanorods, *Biomaterials* 29 (2008) 3743–3749.
- T.D. Zaveri, N.V. Dolgova, B.H. Chu, J. Lee, J. Wong, T.P. Lele, F. Ren, B. G. Keselowsky, Contributions of surface topography and cytotoxicity to the macrophage response to zinc oxide nanorods, *Biomaterials* 31 (2010) 2999–3007.
- S.A. James, B.N. Feltis, M.D. de Jonge, M. Sridhar, J.A. Kimpton, M. Altissimo, S. Mayo, C. Zheng, A. Hastings, D.L. Howard, D.J. Paterson, P.F.A. Wright, G. F. Moorhead, T.W. Turney, J. Fu, Quantification of ZnO nanoparticle uptake, distribution, and dissolution within individual human macrophages, *ACS Nano* 7 (2013) 10621–10635.
- M. Okada, E.S. Hara, A. Yabe, K. Okada, Y. Shibata, Y. Torii, T. Nakano, T. Matsumoto, Titanium as an instant adhesive for biological soft tissue, *Adv. Mater. Interfaces.* 7 (2020) 1902089.
- Y. Zhu, D. Liu, X. Wang, Y. He, W. Luan, F. Qi, J. Ding, Polydopamine-mediated covalent functionalization of collagen on a titanium alloy to promote biocompatibility with soft tissues, *J. Mater. Chem. B* 7 (2019) 2019–2031.
- G.C. Smith, L. Chamberlain, L. Faxious, G.W. Johnston, S. Jin, L.M. Bjursten, Soft tissue response to titanium dioxide nanotube modified implants, *Acta Biomater.* 7 (2011) 3209–3215.
- S. Werner, O. Huck, B. Frisch, D. Vautier, R. Elkaim, J. Voegel, G. Brunel, H. Tenenbaum, The effect of microstructured surfaces and laminin-derived peptide coatings on soft tissue interactions with titanium dental implants, *Biomaterials* 30 (2009) 2291–2301.
- R. Liu, S. Chen, P. Huang, G. Liu, P. Luo, Z. Li, Y. Xiao, Z. Chen, Z. Chen, Immunomodulation-based strategy for improving soft tissue and metal implant integration and its implications in the development of metal soft tissue materials, *Adv. Funct. Mater.* 30 (2020) 1910672.
- S. Lee, B.T. Goh, J. Wolke, H. Tideman, P. Stoelinga, J. Jansen, Soft tissue adaptation to modified titanium surfaces, *J. Biomed. Mater. Res. A* 95A (2010) 543–549.
- G. Sun, Y. Shen, J.W. Harmon, Engineering pro-regenerative hydrogels for scarless wound healing, *Adv. Healthc. Mater.* 7 (2018) 1800016.
- L. Sutrisno, S. Wang, M. Li, Z. Luo, C. Wang, T. Shen, P. Chen, L. Yang, Y. Hu, K. Cai, Construction of three-dimensional net-like polyelectrolyte multilayered nanostructures onto titanium substrates for combined antibacterial and antioxidant applications, *J. Mater. Chem. B* 6 (2018) 5290.
- B.V.O. Muir, D. Myung, W. Knoll, C.W. Frank, Grafting of cross-linked hydrogel networks to titanium surfaces, *ACS Appl. Mater. Interfaces* 6 (2014) 958–966.
- X. Shen, F. Zhang, K. Li, C. Qin, P. Ma, L. Dai, K. Cai, Cecropin B loaded TiO₂ nanotubes coated with hyaluronidase sensitive multilayers for reducing bacterial adhesion, *Mater. Des.* 92 (2016) 1007–1017.
- Z. Yuan, S. Huang, S. Lan, H. Xiong, B. Tao, Y. Ding, Y. Liu, P. Liu, K. Cai, Surface engineering of titanium implants with enzyme-triggered antibacterial properties and enhanced osseointegration in vivo, *J. Mater. Chem. B* 6 (2018) 8090–8104.
- H. Cheng, K. Yue, M. Kazemzadeh-Narbat, Y. Liu, A. Khalilpour, B. Li, Y.S. Zhang, N. Annabi, Ali Khademhosseini, Mussel-inspired multifunctional hydrogel coating for prevention of infections and enhanced osteogenesis, *ACS Appl. Mater. Interfaces* 9 (2017) 11428–11439.
- B. Tao, C. Lin, Y. Deng, Z. Yuan, X. Shen, M. Chen, Y. He, Z. Peng, Y. Hu, K. Cai, Copper-nanoparticle-embedded hydrogel for killing bacteria and promoting wound healing with photothermal therapy, *J. Mater. Chem. B* 7 (2019) 2534–2548.
- G. Eke, N. Mangir, N. Hasirci, S. MacNeil, V. Hasirci, Development of a UV crosslinked biodegradable hydrogel containing adipose derived stem cells to promote vascularization for skin wounds and tissue engineering, *Biomaterials* 129 (2017) 188–198.
- L. Feng, F. He, Y. Dai, B. Liu, G. Yang, S. Gai, N. Niu, R. Lv, C. Li, P. Yang, A versatile near infrared light triggered dual-photosensitizer for synchronous bioimaging and photodynamic therapy, *ACS Appl. Mater. Interfaces* 9 (2017) 12993–13008.
- Z. Feng, X. Liu, L. Tan, Z. Cui, X. Yang, Z. Li, Y. Zheng, K.W.K. Yeung, S. Wu, Electrophoretic deposited stable chitosan@MoS₂ coating with rapid in situ bacteria-killing ability under dual-light irradiation, *Small* 14 (2018) 1704347.
- J. Song, H. Liu, M. Lei, H. Tan, Z. Chen, A. Antoshin, G.F. Payne, X. Qu, C. Liu, Redox-channeling polydopamine-ferrocene (PDA-Fc) coating to confer context-dependent and photothermal antimicrobial activities, *ACS Appl. Mater. Interfaces* 12 (2020) 8915–8928.
- C.M. Shin, J.Y. Lee, J.H. Heo, J.H. Park, C.R. Kim, H. Ryu, J.H. Chang, C.S. Son, W. J. Lee, S.T. Tan, J.L. Zhao, X.W. Sun, Effects of the annealing duration of the ZnO buffer layer on structural and optical properties of ZnO rods grown by a hydrothermal process, *Appl. Surf. Sci.* 255 (2009) 8501–8505.

- [42] J. Kováč Jr, P. Hronec, D. Bůc, J. Škriniarová, P. Šutta, J. Kováč, J. Novák, Study of ZnO nanostructures grown by a hydrothermal process on GaP/ZnO nanowires, *Appl. Surf. Sci.* 337 (2015) 254–258.
- [43] J. Hjortnaes, G. Camci-Unal, J.D. Hutcheson, S.M. Jung, F.J. Schoen, J. Kluin, E. Aikawa, Ali Khademhosseini, Directing valvular interstitial cell myofibroblast-like differentiation in a hybrid hydrogel platform, *Adv. Healthc. Mater.* 4 (2015) 121–130.
- [44] G. Baier, A. Cavallaro, K. Vasilev, V. Mailander, A. Musyanovych, K. Landfester, Enzyme responsive hyaluronic acid nanocapsules containing polyhexanide and their exposure to bacteria to prevent infection, *Biomacromolecules* 14 (2013) 1103–1112.
- [45] S. Haas, N. Hain, M. Raoufi, S. Handschuh-Wang, T. Wang, X. Jiang, H. Schönherr, Enzyme degradable polymersomes from hyaluronic acid-block-poly (ϵ -caprolactone) copolymers for the detection of enzymes of pathogenic bacteria, *Biomacromolecules* 16 (2015) 832–841.
- [46] Y. Wu, Y. Long, Q. Li, S. Han, J. Ma, Y. Yang, H. Gao, Layer-by-Layer (LBL) self-assembled biohybrid nanomaterials for efficient antibacterial applications, *ACS Appl. Mater. Interfaces* 7 (2015) 17255–17263.
- [47] W.L. Hynes, S.L. Walton, Hyaluronidases of gram-positive bacteria, *FEMS, Microbiol. Lett.* 183 (2000) 201–207.
- [48] E. Burello, A.P. Worth, A theoretical framework for predicting the oxidative stress potential of oxide nanoparticles, *Nanotoxicology* 5 (2011) 228–235.
- [49] Q. Naqvi, A. Kanwal, S. Qaseem, M. Naeem, S.R. Ali, M. Shaffique, M. Maqbool, Size-dependent inhibition of bacterial growth by chemically engineered spherical ZnO nanoparticles, *J. Biol. Phys.* 45 (2019) 147–159.
- [50] M. Ramani, S. Ponnusamy, C. Muthamizchelvan, J. Cullen, S. Krishnamurthy, E. Marsili, Morphology-directed synthesis of ZnO nanostructures and their antibacterial activity, *Colloids Surf., B* 105 (2013) 24–30.
- [51] L. Zhang, J. Guo, T. Yan, Y. Han, Fibroblast responses and antibacterial activity of Cu and Zn co-doped TiO₂ for percutaneous implants, *Appl. Surf. Sci.* 434 (2018) 633–642.
- [52] R. McRae, B. Lai, C.J. Fahrni, Subcellular redistribution and mitotic inheritance of transition metals in proliferating mouse fibroblast cells, *Metallomics* 5 (2013) 52–61.
- [53] Y. Ogawa, T. Kawamura, S. Shimada, Zinc and skin biology, *Arch. Biochem. Biophys.* 611 (2016) 113–119.